ZnO-ZnSe Common Cation Heterostructures: *In Situ* Synthesis, Characterization and Photocatalytic Activity

Saba Bashir

NUST201463672MSNS78214F

A thesis submitted in partial fulfillment of requirements for the degree of Master of Science in Chemistry

Supervised by

Dr. Muhammad Fahad Ehsan

Department of Chemistry

School of Natural Sciences

National University of Sciences & Technology

H-12, Islamabad, Pakistan

National University of Sciences & Technology

MS THESIS WORK

We hereby recommend that the dissertation prepared under our supervision by: SABA BASHIR, Regn No. NUST201463672MSNS78214F Titled: ZnO-ZnSe Common Cation Heterostructures: In-Situ Synthesis, Characterization and Photocatalytic Activity be accepted in partial fulfillment of the requirements for the award of **MS** degree.

Examination Committee Members

1. Name: DR. MUHAMMAD ARFAN   Signature: _____

2. Name: DR. SYED RIZWAN HUSSAIN   Signature: _____

3. Name: DR. IFTIKHAR H. GUL   Signature: _____

4. Name: DR. MUHAMMAD NAEEM ASHIQ   Signature: _____

Supervisor's Name: DR. M. FAHAD EHSAN   Signature: _____

_____   25-08-17
Head of Department   Date

COUNTERSINGED

Date: 25/8/17   Dean/Principal

THESIS ACCEPTANCE CERTIFICATE

Certified that final copy of MS thesis written by **Ms. Saba Bashir**, (Registration No. **NUST201463672MSNS78214F**), of **School of Natural Sciences** has been vetted by undersigned, found complete in all respects as per NUST statutes/regulations, is free of plagiarism, errors, and mistakes and is accepted as partial fulfillment for award of MS/M.Phil degree. It is further certified that necessary amendments as pointed out by GEC members and external examiner of the scholar have also been incorporated in the said thesis.
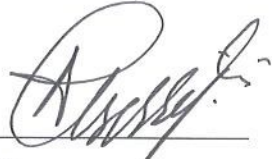
Signature: _____

Name of Supervisor: Dr. M. Fahad Ehsan

Date: 25. 08. 2017

Signature (HoD): _____

Date: 25-08-17

Signature (Dean/Principal): _____

Date: 25/8/17

Acknowledgement

Saba Bashir

List of Abbreviations

ZnO	Zinc Oxide
ZnSe	Zinc Selenide
SEM	Scanning Electron Microscopy
TEM	Transmission Electron Microscopy
EDS	Energy Dispersive X-ray Spectroscopy
UV-vis spectroscopy	Ultra Violet-Visible Spectroscopy
XRD	X-ray Diffraction
e.g.	Example gratia (For example)
i.e.	Id est (That is)
eV	Electron Volts
Nm	Nano-meters
Å	Angstrom
g/mol	Gram per mole
KOH	Potassium Hydroxide
N_2H_4	Hydrazine Hydrate
Se	Selenium
V	Volume
h^+	Hole
NHE	Normal Hydrogen Electrode
CB	Conduction Band
VB	Valence Band
$^\bullet OH$	Hydroxyl Radical
E_g	Energy gap/Band Energy

Abstract

Environmental remediation using sunlight is one of the most promising and cost-effective approaches to mitigate environmental hazards significantly related to the industrial development. In the present work, we reported the synthesis of the common cation ZnO/ZnSe heterostructures via one-pot hydrothermal method at 200 ℃ temperature for 3 hours. The as-synthesized photocatalysts were employed for the photocatalytic degradation of di-azo dye *i.e.* Congo red. XRD spectroscopy was used to analyze the crystal structure, purity and phase of the common cation ZnO/ZnSe heterostructured photocatalysts. Moreover, crystallite sizes and cell volumes of synthesized photocatalysts were also calculated using XRD data. Morphological analysis was carried out via SEM and TEM. The elemental composition in the synthesized photocatalysts was also confirmed using EDX spectroscopy. The alignment of energy levels is an important parameter to determine the pathway of photocatalytic reactions and it was determined with the help of UV-visible spectroscopy as well as XPS analysis from the literature to find the valence band position. Finally, the as-synthesized heterostructures were used for the photocatalytic degradation of Congo red dye under UV-visible irradiation. However, maximum degradation efficiency of 91% in 40 minutes was observed in case of ZnO/ZnSe photocatalysts with 75% ZnSe, respectively. The higher photocatalytic degradation efficiency was attributed to the efficient charge separation as well as the presence of common cation in ZnO/ZnSe heterostructures.

Key words: ZnO, ZnSe, Common cation, Photocatalysis, Congo Red.

Table of Contents

List of Tables

List of Figures

Chapter No. 1: Introduction and Literature Review

1.1 Pollution

Increase in population and human activities not only decreases natural resources but also generates huge amount of wastes which is responsible for the air, water and soil pollution. If not treated properly, this waste causes serious problems to environment and living beings. A **pollutant** might be characterized as any substance accidentally discharged into the environment, which is harmful to the mankind and other living species directly or indirectly and presence of these harmful pollutants or unwanted substances in the environment is called **pollution**[1].

1.2 Types of Pollution

Mainly there might be following types of pollution namely:

- Soil pollution
- Water pollution
- Air pollution
- Noise pollution
- Radioactive pollution

1.2.1 Water Pollution

Water is the basic need of living beings. However, water contamination is an important subject to be faced currently. It can be due to natural events, for example, volcanoes and

earthquake etc. However, main reasons behind water pollution are human activities. This polluted water carries many poisonous and harmful substances such as organic pollutants, metals and solids. Various synthetic substances are very harmful and might cause cancer. If this contaminated water is released in the fresh water, it can be disastrous. Plants can uptake these pollutants and thus these become part of our food as well[2].
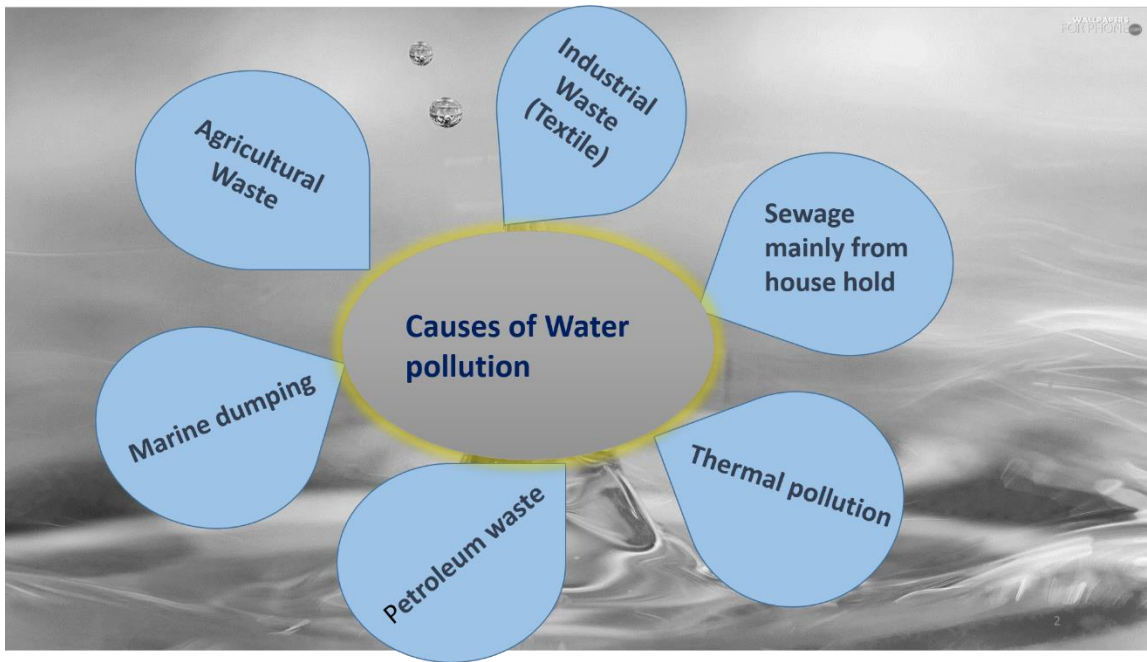
Figure 1.1: Main causes of water pollution.

Mainly water contaminants are characterized in two groups; organic and inorganic water pollutants which are listed in Table.1.1.

Table 1.1: Organic and inorganic water pollutants.

Organic Water Pollutants[3]	Inorganic Water Pollutants[4]
Pathogenic bacteria	Heavy metals e.g. Pb, Zn, Cl, Cu, Fe.
Detergents	Fertilizers such as nitrates and phosphates.
Pharmaceutical drugs	Acidity due to industrial wastes like SO_2.
Herbicides and insecticides	Sulfates SO_4

Waste after food processing	Ammonia
Petroleum oil and fuels	By-products of industries
Textile dyes	Plastic particles
Organic compounds e.g. solvents	Domestic effluents
Trees debris	Shipwreck

1.2.2.1 Effects of Water Pollution

Water containing organic and inorganic pollutants makes it wastewater. Furthermore, presence of colloidal substances makes water cloudy, colored and gives it a bad smell. This colored water does not allow sunlight to pass through it for photosynthesis and inhibit the transfer of oxygen in water. In addition, it also reduces the reproducibility of soil by clogging the pores of soil when permitted to pass through the field. This polluted water also corrodes the sewerage pipes and when mixed with the other drinking water reservoirs, it can be a great threat to living beings.

Water pollution also causes many diseases in humans e.g. cholera, typhoid, skin diseases, kidney problems and diarrhea etc[5, 6].

1.3 Textile Industry Hazards

One of the largest pollution causing industry is textile industry as nearly of 2,000 different chemicals are being utilized in various industrial processes. Water is used in very large quantity from step one till the last step. The water turns out to be enriched with these chemical substances and is then released as contaminated water, which then pollutes the environment through multiple means:

- By heat of effluent
- Increasing pH
- And because it contains color, detergents and numerous other chemicals utilized during the procedure.

The World Bank evaluates that nearly 20% of worldwide industrial water contamination originates from the treatment and coloring of materials. During the process of dyeing not all the molecules of dye are being utilized. These remaining dye stuff, which isn't degraded naturally are then being disposed in water which severely contaminates it. Around 40% of internationally utilized dyes contains naturally bound chlorine, a famous cancer-causing agent[7]. Most abundantly found dyes in wastewater of textile industry are azo-dyes. These are very toxic and difficult to degrade. Toxicity is not due to dye itself but due to its reduction products. The azo bond is very easily breakable segment of an azo dye particle and may effectively experience breakdown by a compound named azo reductase, present in different microorganisms and in almost every mammal including human beings. Many reduction products have been observed to be mutagenic and cancers causing even some were no longer allowed as food dye[8-11].

1.3.1 Textile Organic Dye

The natural and synthetic chemical compounds that make our world polychromatic are commonly known as dyes. The textile dyes which constitute a class of organic compounds, usually referred as the pollutants, expelled in the wastewater are the products of numerous chemical processes in textile industries. The textile coloration industry incorporates various dye houses of multiple sizes that comprehend diverse field of dyes[12].

1.3.1.1 Classification of Textile Organic Dyes

The natural and synthetic dyes are characterized based on their nature and origin. In 2000 BC, the natural dyes obtained by vegetable and animals resources were mainly used in dyeing process and the natural dyes were an integral part of the textile dying industry until 1856. Phoenician has also been found to be well-aware of the dyes. They were using tyrian purple and indigo dye extracted from crushed sea snails and indigo plant in the 15th century BC and 3000 BC, respectively. The clothes of Egyptian mummies were wrapped and dyed using the dyes produced from the madder plant. The discovery of synthetic dyes took place

in 1856 with synthesis of mauve dye (aniline) by H.W. Perkin (UK). Later in 1956 P. Garis coined diazotization reaction led to the synthesis of azo dyes.

The chemical structure of dyes is related to aromatic compounds that contain aromatic rings with several functional groups and delocalized electrons. Chromogen-Chromophore structure (electron acceptor) impart color to the dyes, whereas, its dying strength is the result of auxochrome group (donor of electron) in its chemical structure. The chromogen contains the rings of benzene, naphthalene or anthracene, and binding chromophores that constitute double conjugated connection with delocalized electrons. The chromophore structure is exhibited by different functional groups including the azo $(-N=N-)$, ethylene $(=C=C=)$, carbonyl, carbon-nitrogen $(=C=NH;-CH=N-)$, methyn group $(-CH=)$, carbon-sulfur and nitro $(-NO_2;-NO-OH)$. While the auxochrome that grants binding strength to the dyes are mainly composed of $(-NH_2, -COOH, -SO_3H$ and $-OH)$[13].

1.3.1.2 Characterization of Textile Dyes

To identify an unknown dye, we need to employ a few special analytical processes (*i.e.* coupled spectrophotometry, mass spectrometry technique and gas/liquid chromatography). The identification of the dye in the dying process should follow the following steps:

- ❖ Identifying the physio-chemical characteristics of the dye (*i.e.* boiling-point, solubility of water, relative density, partition coefficient, volatility, vapor pressure, oxidative characteristics and size distribution etc.)
- ❖ Observing toxicological properties (*i.e.* severe oral-toxicity, inhalation, eyes and skin irritation and sensitivity of skin.)
- ❖ Checking the ecotoxicological characteristics (*i.e.* serious effect to aquatic life, daphnia, bacteriological inhibition, degradation: ready biodegradability).

❖ Synthesis information *i.e.* synthesis method, concentration and quantity, storage and precautions.

Due to the presence of an electron pair on the nitrogen, azo dyes can gain proton and hence its reactivity is due to the interaction of free electron pairs with the delocalized π orbitals. The basicity of the aminic group is diminished due to the attachment of acceptor group −Cl or −NO_2. Similarly, the presence of the donor group −CH_3 or −OR on aromatic rings increases the basic character of the aromatic amine group. The presence of hydroxyl group, carboxyl or sulfoxyl imparts amphoteric properties to azo group.

1.3.1.3 Environmental Hazards and Effects of Azo Dyes

Azo dyes used in textile industry are mainly nitrogenous based compounds. Azo dyes may disintegrate under specific conditions to form cancer causing and allergic aromatic amines. Widely spread textile industry is the crucial source of contaminants expelled in wastewater that contains byproducts like water soluble dye residues and become part of environmental entities (soil, air and water). Among all the textile colorants, Azo and anthraquinone are the two most widely used in textile industry. Metal-complexed dyes are preferably used because of their high stability attributed to consistent exposure to the water and sunlight. Due to their highly effective stability, these dyes are mostly found in fresh water bodies (rivers), where they are the main reason of various toxicological impacts to the aquatic ecosystem. These dyes are very stable in nature (having half-lives of 2-13 years), and they have been found in rivers worldwide[14].These dyes contain some metal coordination complexes *i.e.* cobalt, chromium or copper, which have already been designated as the highly hazardous pollutant for environment. Moreover, these dyes are mutagenic due to azo and aromatic groups. An experiment was carried out by F. Copaciu to show the harmful effects of two anthraquinone dyes (OB and LB) and four azo dyes (LR, NR, NDB, LDB) on the growth and properties of plants[15]. For instance, the most basic biological process, photosynthesis, has been found to be reduced by the presence of these dyes in the

water. Furthermore, there are several other sources (*e.g.* textile industries, pharmaceutical paper, pulp, dye intermediates industries, and craft bleaching industries etc.) that are found to be the basic cause of production of these dyes in the natural water bodies. It has been found that 10-25% textile dyes used during the dying process and 2-20% of them are directly expelled to the fresh water bodies. As discussed above, these dyes in the wastewater are not treated well and have harmful effects on the aquatic life on longer exposure. For example, optimum condition for hydrolyzed reactive blue 19 is (pH=7 and 25 ºC. Hence it can remain in water for up to 46 years. Therefore, the dye containing wastewater should be treated as per proper environmental standards. This dye containing wastewater can be treated using different process that include non-biological (i.e. Specific physical, chemical, electro-chemical processes, etc.) and biological treatment.[7]

1.4 Separation and Elimination of Organic Wastes from Water Bodies

The organic textile dyes are removed from water particularly from industrial wastewater using efficient methods following two diverse processes:

1) Elimination of organic pollutant.
2) The semi or full degradation or decomposition of organic effluents.

Elimination technique corresponds to fluid (centrifugation, filtration process, sedimentation technique, and flotation) or on membranes (ultra, Nano-filtration, micro and reverse osmosis). In addition, Physical and chemical methods (*i.e.* precipitation, coagulation-flocculation, adsorption and ionic exchange) can be employed to remove solidified compounds from water[16, 17].

Pollutants can also be eliminated using biological and physio-chemical treatment methods including adsorption, coagulation-flocculation (with inorganic coagulants and organic polymers), chemical oxidation, ozonation and electrochemical processes etc[18-20].

1.4.1 Physical and Chemical Treatment Methods

The de-colorization separation process can be categorized into two major steps. The first step corresponds to the removal of solid and un-soluble impurities. The later step involves the removal of extra pollutants when converted into solid form. Various current and emerging dye separation and elimination techniques applied for textile wastewater with their basic advantages and restraints are given below in Table 2.2.

Table 2.2: Various separation techniques for textile wastewater and their advantages and disadvantages.

Treatment methodology	Advantages	Dis-advantages
Electro-kinetic coagulation[21]	• Economical	• Huge sludge formation
Ozonation[22]	• Efficient in azo dye separation. • No volume change as works in gaseous state.	• For dispersed dyes, it is not applicable. • Discharge aromatic dyes. having small half-life of ozone i.e. 20 mins
Ion exchange	• Regeneration with low loss of adsorbents	• Specific application; not effective for all dyes
Activated charcoal[23]	• Economical. • Good separation efficiency over wide variety of dyes	• Very costly.
Precipitation, coagulation-flocculation[17]	• Less detention time and inexpensive. • Comparatively good removal efficiencies.	• Clumps removal and treatment. • Specific operating conditions.

Ashes of coal[24]	• Economically attractive. • Better separation efficiency.	• Large amounts and maximum contact time required. • Less efficient than activated charcoal.
Wood sawdust /chips[25]	• Efficient adsorbent. • Cost effective. better adsorption capacity specially towards acid dyes.	• Large amounts long retention time required.
Electrochemical oxidation[26]	• Non-toxic end products	• Cost intensive; high electricity cost required.
Irradiation	• Better efficiency and oxidation.	• Requires huge amount of Oxygen.
Photochemical methods[27]	• No formation of sludge	• Side reactions.
NaOCl oxidation	• Low temperature requirement. • Effective for azo dyes degradation.	• Expensive method. • Releases aromatic amines.
Silica gels[28]	• Effectively remove basic dyes	• Side products reduce efficiency

1.4.2 Biological Treatment Methods

Free oxygen depending method[29]	• Separate all dyes	• Expensive
Anaerobic methods	• Show resistance to many complex dyed compounds.	• Slow growth rate and long detention time

Using Fungal, Algal & Bacterial cell	• Good efficiency for fewer amounts.	• Cost exhaustive.
	.	

1.4.3 Advanced Treatment Methods

Advanced oxidative methods	• Full degradation occurs. • Efficient method increases biodegradability.	• Expensive
Filtration (membrane)[30]	• Efficiency and reusability.	• Expensive. Sludge formation. • Do not remove dissolve solid particles.
Photocatalysis[31]	• Normal conditions required. • Non -toxic and cost effective. Complete degradation with shorter detention time.	• Effective for small quantity of dyed compounds.
Sonication[32]	• Simple method. • Very efficient.	• Newly developed method further applications yet to be found.

Treatment through enzymes[33]	• Effective for only specific compounds. • Independent of contact times.	• Separation and purification of enzyme is difficult.
Engineered wetland systems[34]	• Economically attractive and can be applied of large amount of wastewater.	• Very expensive • And requires high competency in treatment.

1.4.4 Physical Treatments

1.4.4.1 Adsorption

In this method, the soluble organic dyes are shifted from water to the solid surface using adsorbent. The absorbent can absorb these waste materials up to a certain capability after which it must be replaced with the new material.

It is the most inexpensive process to eliminate these dyes using two simplified processes; *i.e.* adsorption and ion exchange.

1.4.4.2 Irradiation

In irradiation process, a beam of electron or gamma rays is used to separate organic toxic compound and detoxifying microorganisms.

1.4.4.3 Membrane Processes

In this process, a selectively permeable membrane is used to eliminate the pollutants and dyes from wastewater with varying pressure. This method includes; ultra-filtration, nano-filtration, micro-filtration and reverse osmosis.

1.4.5 Chemical Treatments

1.4.5.1 Oxidative Procedures

Chemical oxidation degrades harmful compounds into less toxic substances.

1.4.5.2 Ozonation Process

Using ozone as oxidizing agent, the aromatic rings of the textile dyes are broken down and other effluents are degraded. Ozone can interact with dye molecules directly or indirectly.

1.4.5.3 Photochemical Oxidation

Mixing H_2O_2 with wastewaters under ultra violet rays on it can disintegrate the dye compounds to the small compounds like CO_2 and H_2O.

1.4.6 Electrochemical Process

In this process, for complete oxidation of pollutants electrical energy is applied on the anodes of high oxidation power. It has following advantages:

    i)   Reduction of diff types of effluents.

    ii)   It can be applied with different volume concentrations.

The disadvantage is the formation of metallic hydroxide sludge.

1.4.6.1 Coagulation–Flocculation and Precipitation

This method is based on the principle of electrostatic attraction among oppositely charged soluble dye and polymer molecules.

1.4.7 Biological Treatment

1.4.7.1 Aerobic Biological Treatment

In this treatment, biodegradation of organic compounds is carried out using bacteria fungi and algae (*e.g.* Chlorella and oscillotoria species).

These microorganisms degrade these pollutants using enzymes lignin peroxidases (LiP) and with the manganese dependent peroxidases (MnP).

1.4.7.2 Anaerobic Biological Treatment

Anaerobic bio-degradation of azo dyes follows these steps:

    i)   Redox reaction of azo dyes in wastewater with hydrogen.

    ii)   Methane formation.

    iii)   Release of electrons.

Azo bonds are broken due to the reaction of released electrons with the dye, thereby decolorizing the wastewater.

1.5 Advanced Oxidation Processes (AOPs)

Advance oxidative processes are series of chemical reactions responsible to produce powerful oxidizing agents. H_4RnO_6 and xenon fluoride (XeF) are known to be the strongest oxidizing agent but these are not commercially suitable for the water purification as they are very reactive and form toxic intermediates. Similarly, oxidizing agent which are halogen based are not useful as they halogenate the organic compound and form harmful products. Mostly, heavy metal based oxidizing agents have the same problem of toxicity. So, they cannot be used as well e.g. dichromate $Cr_2O_7^{-2}$.

Oxidizing agents like hydroxyl (•OH), (O_3) elemental oxygen (O) and hydrogen peroxide *i.e.* H_2O_2 are considers as most favorable in this regard.

Table 1.3: Standard reduction potential values for some oxidizers at T=298.15 K, for acidic conditions at pH =0[35].

Reduction half-cell reaction	E° (V) vs. SHE
$XeF + e^- \rightarrow Xe + F^-$	3.40
$2OF_2(g) + 4H^+ + 4e^- \rightarrow O_2(g) + 4HF$	3.29

$OH^- + H^+ + e^- \rightarrow H_2O$	2.56
$O(g) + 2H^+ + 2e^- \rightarrow H_2O$	2.43
$O_3 + 2H^+ + 2e^- \rightarrow O_2 + H_2O$	2.08
$H_2O_2 + 2H^+ + 2e^- \rightarrow 2H_2O$	1.76
$HCIO_2 + 2H^+ + 2e^- \rightarrow HCIO + H_2O$	1.67
$HO_2 + H^+ + e^- \rightarrow H_2O_2$	1.44
$Cl_2 + 2e^- \rightarrow 2CI^-$	1.40

1.5.1 Photocatalysis

Landau was the first person who used the word photocatalyst in 1913[36].The first report was by Fujishima and Honda[37] in utilization of TiO₂ for water splitting. Their work attracted attention globally and triggered many research activities. Photocatalysis refers to the process in which a solid material, termed as the photocatalyst takes part in the reaction by photoabsorption. This process increases the rate of photochemical reaction in the presence of a photocatalyst. Chemical composition of the photocatalyst remains unchanged during the chemical process. The selection of photocatalyst is very critical. It is not compulsory for a solid material to function as photocatalyst in all photo-catalytic reactions. Therefore, we can say that photocatalyst is not a substance that can only be synthesized rather it is designed and developed.

Photocatalysis has two main types:

    i)   **Homogenous photocatalysis.**

    ii)   **Heterogeneous photocatalysis.**

The main difference between these two types is that the reactants and the photocatalyst are in the same phase in case of homogenous photocatalysis while both are in different phase in heterogenous photocatalysis. Heterogeneous photocatalysis involve complex reaction sequences mainly based on 5 following steps:[38]

1- Mass exchange of organic pollutants to the top of catalyst in liquid phase.

2- Organic pollutants get adsorbed on the activated photocatalyst surface.

3- Photocatalytic reaction takes place on catalyst surface.

4- Intermediate compound then desorbs from catalyst surface.

5- Intermediate then transfers from interface region to the mass liquid.

1.5.2 Characteristics of a Good Photocatalyst[39]

Good photocatalyst must possess following characteristics:

- ➢ Light active
- ➢ Photo stable
- ➢ Chemically non-reactive
- ➢ They should be of low cost and non-toxic
- ➢ Photocatalyst should be recovered at the end and can be recycled

1.5.3 Basic Principle of Photocatalysis

Photocatalysis is started by electron-void couples after band gap excitation. The difference of energy between conduction band and valence band is called "band gap". When a photocatalyst is irradiated by light of energy equivalent to or more than band-gap energy, the electrons present in outermost band can be excited to the conduction band and void with positive charge is created. This is photoexcited state of semiconductor[40].These photogenerated electron-hole pairs can recombine with the release of energy in the form of heat and with no chemical change. If they do not recombine they induce oxidation and reduction processes in water[41]. For photocatalytic water/air treatment, valence band (VB) holes are the essential components that prompt the oxidative disintegration of environmental toxins as shown in Fig. 1.2.
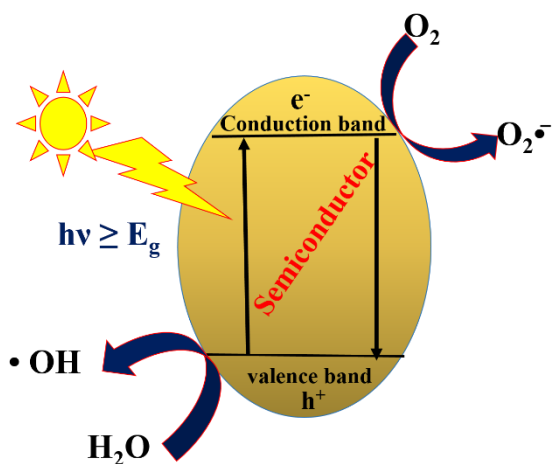
Figure 1.2: General photocatalysis mechanism over semiconductor photocatalyst.

These positive holes react in either ways *i.e.* directly attacking the pollutant or reaction with water and forming hydroxyl radical (•OH) which is very strong oxidant and it has oxidation potential 2.8 V (NHE). This hydroxyl radical will quickly strike the pollutants on the top and will convert them into CO_2 and H_2O on complete degradation. On the other hand, electron will combine with oxygen and produce superoxide anion. And in the presence of light this cycle keeps going (Fig. 1.2). Different metal oxides[42-44] and sulphides[45, 46] are used as photocatalysts *e.g.* TiO_2[47], ZnO[48, 49], WO_3[50], CdS[51], CeO_2 [52], Fe_2O_3[53] etc.

1.6 Metal Oxides as Photocatalysts

Oxides of different metals *e.g.* titanium, zinc, iron, tin, vanadium, cerium and cadmium are used as photocatalysts. These photocatalysts work on same basic principle in which they absorb light either UV or visible or both and become activated and form electrons and holes. These holes will then further degrade the pollutants. Among many other photocatalysts ZnO and TiO_2 extensively used. Metal oxides have many applications some of them are given as follow:
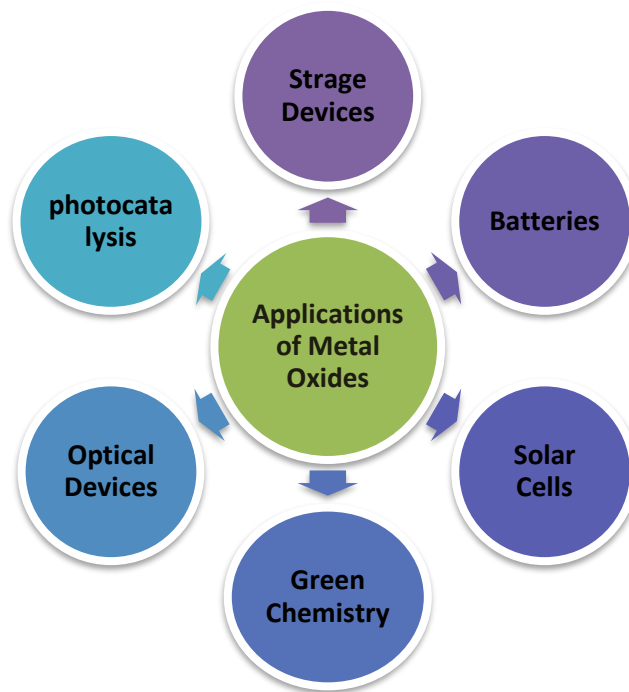
Figure 1.3: General applications of metal oxides.

Some of the metal oxide cannot be efficiently be used as photocatalysts due to their limited light response, large band gap and electron hole recombination. In order to overcome these problems metal oxides are combined with other metals and semiconductors so the band gap is reduced and so as the electron hole recombination and photocatalyst utilizes large portion of light[42].

1.7 ZnO as Photocatalyst

It is somehow not easy to search non-poisonous and stable semiconductors nanomaterials which have high efficiency of photocatalytic degradation of contaminants. However, TiO_2 and ZnO are widely used in this regard. Comparing with TiO_2 nanostructure ZnO has gained more consideration because of high quantum effectiveness, inexpensive, heat stability, chemical strength, non-toxic and high availability. So, ZnO seems to be a vital

and favorable metal oxide as photocatalyst, it is semiconductor and have large band gap 3.37 eV. It has large exciton binding energy almost 60 meV. Its electron mobility is (205-300cm2V/s) much greater than TiO$_2$ which has (0.1-4cm2V/s)[54]. Another advantage of ZnO is it can easily be synthesized under mild conditions and it also act as germicide. It is used in nanosized form due to 2 main reasons including (1) high surface area, (2) effect of quantum confinement in nano-size materials. Moreover, for photocatalysis process material need to absorb the incidents light and create electron and hole through excitation of energy band gap without scattering and blocking the light. It can only be possible if the nanoscale semiconductor is used which have reasonable energy of band gap[55].so many dyes can be degraded using ZnO photocatalyst like methyl orange (MO), reactive orange 16, eosin y, methylene blue (MB)[56], an azo dye acid red 27[57], many other commercial azo dyes like remazol brilliant orange 3R (C.I. reactive orange 16) and remazol brilliant red F3B (C.I. reactive red 180)[58]. However, when exposed to UV-light, ZnO suffers via rapid electron-hole recombination which affects the overall photocatalytic efficiency. To overcome this issue, one approach is introduction of anionic non-metal dopant to ZnO like C, S or N[59]. However, the formation of various sites than act as recombination centers and, hence, hamper the overall photocatalytic activity Therefore, we have designed coupling of two semiconductors for higher activities[60, 61].

1.8 Heterostructures for Photocatalytic Degradation

Many other nanocomposite photocatalysts have already been reported for degradation of dye like Mingce Long et al[62] presented and discussed synthesis of Co$_3$O$_4$/BiVO$_4$ composite by impregnation technique. Different characterizing techniques like XRD, BET surface area, TEM and UV-visible diffuse reflectance spectra were used to characterized the catalyst. After calcination BiVO$_4$ kept its structure white Co is available as Co$_3$O$_4$ and scatters on the surface of BiVO$_4$ to form the heterojunction composite. The photocatalytic activity was being examined on phenol. The composite photocatalyst shows improved

photocatalytic action in visible light. The efficiency of the catalyst noticed maximum when amount of Co is 0.8 wt. % and calcined temp was 300 ºC. The improved action is related to the p-n heterojunction semiconductor frame and the reducing recombination of hole-electron pairs produced by irradiation of light. The composite photocatalyst is very useful for water cleansing purpose for its great precipitation execution and stability.

Xia Hui-li et al[63] prepared a novel composite oxide $CuO-SnO_2$ by co precipitation technique and further characterized by XRD, TEM and N_2 adsorption-desorption measurement. The photocatalytic action of composite $CuO-SnO_2$, assessed by the photodegradation of acid blue 62 as a test response under the illumination of Xenon light and activity is also affected by calcined temperature and molar ratio of Cu to Sn. Maximum photocatalytic activity was found when 3 hrs. calcination done under 500 ºC temp. When compared to P25 TiO_2 the $CuO-SnO_2$ exhibited improved photocatalytic action.

H. Seema et al[64] synthesized a photocatalyst $RGO–SnO_2$ by redox reaction among rGO and $SnCl_2$. Graphene oxide (GO) reduced while Sn^{+2} become oxidized into RGO and SnO_2 results in homogenous distribution of SnO_2 on reduced graphene oxide sheets. Its uniform distribution was confirmed by SEM and TEM images. Their average particle size that is 3-5 nm was confirmed by high-resolution transmission electron microscopy (HRTEM). This formed composite exhibit elevated photocatalytic action when used on methylene blue under sun light when compared to bare SO_2. Results showed that this photo catalyst could be used on other organic dyes as well to degrade them.

Yao Wu et al[65] reported ZnO/CdSe heterostructure photocatalyst in which CdSe nanoparticles were scattered on the ZnO plates by facile solution method. Hybrid samples were analyzed by XRD, SEM, TEM and UV–vis absorption spectrum. Photocatalytic action of ZnO/CdSe heterostructure shows enhanced photocatalytic proficiency compared to ZnO. CdSe acts as photosensitizers to enhance absorption spectrum toward visible light

zone. As CdSe dispersion helped to reduce electron and holes recombination and increased photodegradation activity.

A.Ye et al[66] reported CdS–graphene by hydrothermal process for methyl orange (MO) degradation under visible light illumination. They compared its efficiency with CdS–CNT and found CdS–graphene composite more efficient photocatalyst because of greater contact interface which efficiently increases movement of electrons from CdS to GR.

M. Vinothkannan et al[67] proposed one pot synthesis route for reduced graphene oxide (RGO)/Fe_3O_4 nanocomposites and solanum trilobatum used as reducing agent. To increase thermal stability of GO, hydrophilic group was removed. Methylene blue was degraded to measure its photocatalytic efficiency. Due to increased number or active sites methylene blue was fully degraded in 12 minutes.

W. Dong et al[68] designed 2-D hexagonal TiO_2–SiO_2 mesoporous nanocomposites. SiO_2 provides better adsorption centers being excellent adsorbent for pollutants while TiO_2 acts as photocatalyst to degrade these adsorbed pollutants. To check photocatalytic action and adsorption performance cationic rhodamine-B (RhB) was degraded successfully.

Similarly, N. karamat et al[69] synthesizes $LaSmTiZrO_7$ microemulsion method and SnSe through hydrothermal method then they formed its composite again using hydrothermal process. This composite was then applied for foron blue dye degradation under visible light illumination. Heterostructure formation minimized electron-hole recombination and exhibited better photocatalytic efficiency than its bare components.

1.9 ZnO Heterostructures for Azo Dyes Degradation

J. Saffari et al[70] synthesized Fe_3O_4/ZnO nanocomposite through surfactant-free sonochemical method in water. They studied sonication time and power effect on particle

size and morphology. Afterwards, used this heterostructure for degradation of eight dyes (*i.e.* methyl orange, methylene blue, rhodhamine b, eosin y, acid brown 14, acid blue 92, acid red 151 and acid violet 7) all dyes were sufficiently degraded. Maximum degradation was observed of methyl orange *i.e.* 94% and minimum was of methyl blue 18% in 60 minutes. It also exhibited magnetic properties.

M. Bagheri et al[71] reported $CuInSe_2$–ZnO photocatalyst synthesized through solvothermal process. The composite showed absorption in visible region. Then their photocatalytic efficiency was evaluated by degradation of Congo red dye. Highest removal percentage was calculated as 99.8% after 90 mins under UV-Visible irradiation with 10 wt. % $CuInSe_2$.

Benxia Li. et al[72] synthesized efficient photocatalyst ZnO/graphene-oxide (ZnO/GO) by facile chemical deposition method. GO have high porosity and high surface area beneficial for dye absorption and oxygen mass transfer. Composite showed much greater photocatalytic efficiency than its bare components. Efficiency further improved on annealing in N_2 environment due to suppressed electron hole recombination in methylene blue degradation.

M. Pirhashemi. et al[73] prepared AgBr–ZnO through refluxing for 3 hours at 90°C AgBr was loaded on hexagonal wurtzite ZnO. Then photocatalytic action was carried out at methylene blue and successfully degraded.

 Similarly, B. Pant. et al[74] reported TiO_2/ZnO decorated with carbon nanofibers by electrospinning technique then hydrothermal and calcination. After characterized through different techniques the photocatalytic activity was evaluated by methylene blue degradation furthermore, antibacterial activity was also studied. Increased photocatalytic action of composite was mainly because of adsorption property of carbon nanofibers. This photocatalyst was proved to be stable and completely recovered at the end of the process.

R. Saravanan et al[75] degraded methylene blue and methyl orange using different concentration of photocatalyst under visible light irradiation. Catalyst ZnO/CuO was prepared through thermal decomposition method. After characterization, the composite which was most photocatalytically active was applied for textile dyes degradation and measured activity. ZnO/CuO composite with ratio (95:5) exhibited highest degradation efficiency *i.e.* 97% for methylene blue and 87% for methyl orange after 120 minutes.

M. Faisal et al[76] synthesized $ZnO-CeO_2$ by low temperature process. As synthesized photocatalyst were then used for the degradation of acridine orange and methylene blue. Degradation efficiency was 84.55% and 48.65% in 170 minutes. Composite was found to be very efficient and sensitive.

M. Goodarzi et al[77] reported $CaFe_2O_4$–ZnO nanocomposites synthesis and their bare components of different morphologies using hydrothermal method. They studied effect of different parameters on particle size of products like capping agents, concentration, precipitating agent and time of reaction. Starch and glucose were used as capping agent as they are safe and inexpensive. Synthesized products were characterized by different techniques like SEM, XRD and FTIR. Three azo dyes were used to evaluate their photocatalytic activity those were acid violet, acid black and acid brown under UV irradiation. $CaFe_2O_4$–ZnO nanocomposite exhibited very suitable and efficient degradation and magnetic properties then its individual components.

Md. Tamez Uddin et al[78] prepared SnO_2−ZnO heterojunction photocatalyst by 2 step method, in first step they synthesized SnO_2 through precipitation and hydrothermal methods while in second step SnO_2 was reacted with zinc acetate and then sample was referred to calcination at 500 °C. Final product was confirmed by different techniques including XRD, XPS, Raman spectroscopy, FTIR, TEM and UV- spectroscopy. This heterostructure exhibited good photocatalytic efficiency in the degradation of methylene blue than individual ZnO and SnO_2 this efficiency was attributed to the better charge

separation and reduced recombination. They also evaluated the stability of photocatalysts and found out that it can be recycled many times.

1.10 ZnSe/ZnO Photocatalysts

For coupling with ZnO to avoid electron/hole recombination, semiconductors with narrow energy band gaps are preferred like CdS and CdSe are being used earlier but it has limitation that they are cancer causing. Other metal sulfides and α-Fe_2O_3 encounter corrosion on their electrodes.

ZnSe is an important n-type semiconductor having energy band gap of 2.67 eV. It is used in many optical instruments, diodes, and light detectors, also works as scintillators and show peak of emission at 640nm and is one of the most reliable photocatalyst as well. It also can degrade many dyes some of them are; methylene blue, ethyl violet, acid yellow 17 azo dye.[79] Due to these properties and small band gap we coupled ZnSe with ZnO. So, band gap of ZnO is reduced and its photocatalytic activity is considerably enhanced. We synthesized ZnO-ZnSe composite by hydrothermal route. This composite gives a good route to the separation to hole and electron couple and make an effective system to degrade organic pollutants in waste water.

Synthesis of ZnO/ZnSe composite has already been reported but still not enough work has been done in this regard. H. Liu et al in 2015,[80] reported that Porous ZnO/ZnSe heterostructures were prepared by ultrasonic irradiation method and also from in situ ion exchange reaction. Synthesized ZnO/ZnSe heterostructures were spherical in shape showed much increased visible light photocatalytic action over ZnO microspheres due to the vast surface region and the distinct heterostructure, which supports the detachment of photo-induced electrons and holes transport inside the catalyst. ZnO/ZnSe heterostructure produced with different amount of ZnSe showed different photocatalytic action when tested for the degradation of methylene blue. For the determination of photocatalytic activity, quantity of ZnSe played a vital role.

S. Cho et al in 2011,[81] reported a method for synthesis of 3D ZnO/ZnSe type II surface-modification reactions which were solution based. ZnO/ZnSe heterostructures ware formed through dissolution-recrystallization mechanism. The product showed absorption in visible region. Photocatalytic activities of both pure 3D ZnO and 3D ZnO/ZnSe were investigated. The visible light photocatalytic actions of 3D ZnO/ZnSe heterostructures were quite greater than pure 3D ZnO this was due to ZnSe nanoparticles enhanced absorption of visible and increases charge-carrier transfer of ZnO/ZnSe heterostructures. Both the photocatalysts exhibited different activities in visible light by changing their structures as surface modifications played very important role in this regard. They suggested that this surface modification procedure can be used for the formation or ZnO/ZnSe heterostructure arrangements for their application in different purposes like solar cells and splitting of water by photochemical method.

K. Wang et al in 2008[82] synthesized ZnO/ZnSe core/shells nanowires which were of large area, properly oriented and are not affected by air. They were directly synthesized on transparent conducting oxide (TCO) substrate by joining two techniques *i.e.* chemical vapor deposition (CVD) and PLD *i.e.* pulsed lased deposition. Later, products were investigated by different characterization techniques. SEM and TEM used for morphological studies which confirmed that ZnO nanowires were monotonously and vertically developed on TCO substrate while ZnSe which has 5-8 nm thickness developed on ZnO nanowires. Further studies explained that ZnO/ZnSe core/shells nanowires showed absorption band in region lower than the band gap of ZnO. This ZnO/ZnSe core/shells can be applied in solar cells.

S. Cho in 2012[83] reported synthesis of ZnO-ZnSe heterostructure is visible light active photocatalyst. Porous ZnO were prepared through hydrothermal reaction which is microwave assisted and then through dissolution recrystallization method this porous ZnO was transformed into ZnO-ZnSe nanocomposite using selenium ion aqueous solution.

Nano crystallites of both ZnO and ZnSe were well mixed specially at surface. This porous ZnO-ZnSe nanocomposite exhibited much greater photocatalytic activity than porous ZnO. Enhanced photocatalytic activity of our nanocomposite suggested that it can be used in solar cells.

W. Chen et al[84] synthesized ZnO/ZnSe core/shells heterostructures with different amount of both components were synthesized by CVD (chemical vapor deposition) method under different temperatures in two steps.

However, all these methods were costly and time consuming. We formulated one-pot synthesis route for the formation of ZnO/ZnSe nanocomposite. Then the as-synthesized composite heterostructure was employed for the photocatalytic mineralization of Congo red dye.

1.11 Congo Red Dye

Congo red has molecular formula $C_{32}H_{22}N_6Na_2O_6S_2$ (molecular weight 697 g/mol) it is water soluble secondary diazo dye gives red color solution. It is more soluble in organic solvents. First synthesized by Paul Böttiger in 188[85].It also has property of aggregate formation in organic solutions and water. It has many applications in textile, paper, lather industry and used for diagnostic purposes. Congo red is now banned in most of the industries as it is considered as mutagen and carcinogenic[86]. Further effects on human includes, skin or eye irritation and allergic reaction when in contact and if swallowed in large amount it can cause vomiting, gastrointestinal tract irritation and can also effect blood[87]. When released from textile industries in water it gives red color in water and inhibits the sun light to pass through water so restricts the photosynthesis process. Due to its complex structure, it is a stable compound and difficult to degrade.
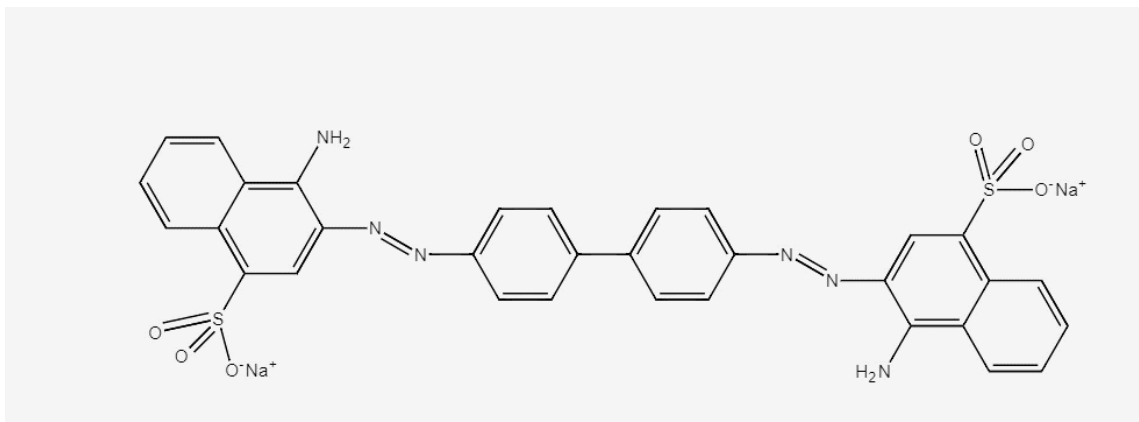
Figure 1.4: Congo red dye structure.

1.12 Pollutant Degradation and Hydrogen Production over Nanocomposites

Young-jin cho et al[88] designed and synthesized Pt/GO/TiO$_2$-F composite which permits the H generation along with the degradation of 4 chlorophenol. H generation capability of composite with 3 components *i.e.* Pt/GO/TiO$_2$-F was greater than TiO$_2$ based binary components composites. Graphene oxide (GO) deposition on TiO$_2$ greatly increases the Fe^{3+} mediated photocurrent. But GO positive effect on dual photocatalytic action can only be observed when fluoride and Pt were also present. As GO accelerate the movement of electron to the Pt while surface fluoride reduces the electron-hole recombination. They also proposed that if surface fluoride is replaced by phosphate still GO shows positive effect. Moreover, ternary composite was stable throughout the degradation and H$_2$ production process.

Xi Wang at al[89] proposed CdS-ZnS photocatalyst synthesized by stepped micro emulsion process. This composite had potential to degrade organic materials simultaneously generate photocatalytic hydrogen in visible light irradiation. Deposition of ZnS decreases the recombination of holes and electrons produced on CdS results in speedy hydrogen production compared to CdS. Sensitivity of CdS was protected by ZnS coating and greatly

enhances its strength against photocorrosion. Organic materials containing ethanol, formic acid and methanol permit the generation of hydrogen under visible light. Highest hydrogen generation rate was attained this composite in formic acid solution at 266 ± 4 mm/m²-h with the efficiency of $3.05 \pm 0.05\%$ photo energy conversion. Along with the production of hydrogen, the relative rate of photocatalytic degradation of organics was 4272 ± 67 mg COD/m²-h.

S. Martha et al[90] proposed photocatalyst V_2O_5/N, S- TiO_2 synthesized by solid state reaction method. Synthesized material was characterized by different techniques *i.e.* XRD, BET, XPS, UV-VIS, FTIR, SEM, and TEM. Photocatalytic use of photocatalytic material was assessed for hydrogen generation under visible light illumination and photodegradation of phenol. V_2O_5 constituent had vital role in photocatalytic action at longer wavelength. V_2O_5/N, S-TiO_2 exhibited much better action in production of hydrogen using visible light and 88% degradation of 100 mgL^{-1} solution of phenol using direct solar light within 4 hrs.

Vasileia M. et al[91] reported Pt/CdS/TiO_2 photocatalysts used as both immobilized and powdered and attempted to degrade both organic as well as inorganic pollutants in water. It has been found that the accumulation of Pt on powdered joined with CdS/TiO_2 semiconductors creates photocatalysts that could totally oxidize inorganic particles and generate hydrogen however couldn't effectively degrade organic material while separately deposited Pt and CdS/TiO_2 on fluorine doped tin oxide (FTO) electrode, results in effective ethanol photodegradation but not efficient with Na_2SO_3 and Na_2S.

X. Zhang et al[92] used photocatalyst 3%WOx/TiO_2 for degradation and hydrogen production purposes. They degraded 2 aromatic contaminants under visible light that is 4-chlorophenol as well as 2,4-dichlorophenoxy acetic acid and it has been found that degradation of as 2,4-dichlorophenoxy acetic acid occur more quickly with greater amount of hydrogen production than 4-chlorophenol. This happened because they both have

different potential of oxidation, hydrophobic impacts and electrostatic cooperation with the photocatalyst 3%WO_x/TiO_2.

J. Xu et al[93] discussed MoS_2/CdS photocatalyst for production of hydrogen and composite was synthesized by hydrothermal method. Its surface and crystal morphology was then examined by SEM, TEM, HRTEM, XRD and other characterization techniques were also applied and results showed that MoS_2 was evenly distributed on CdS surface. This coupling helped in enhancement of photocatalytic action. 2wt% of MoS_2 loaded on CdS surface then rate of hydrogen production was increased by17 times. And maximum hydrogen evolution by this composite was recorded 4.06 mmolg-1h-1.

Li Jia et al[94] synthesized number of (N-graphene)/CdS nanocomposites for water splitting. It was found to be a very efficient photocatalyst for production of hydrogen under visible light irradiation. With the amount of 2 wt. %N-graphene doping this photocatalyst showed highest photocatalytic action. Their studies are also important regarding concept of specific junction structure between co-catalyst and semiconductor for better photocatalytic activity. According to them N- graphene as co-catalyst had many merits like it protects CdS from photocorrosion, also served as charge collector and lastly it made hydrogen production easier. Their finding was initiating point for N-doped graphene as co-catalyst for different semiconductors to produce hydrogen.

Takuya Miwa et al[95] discussed hydrogen production through photocatalyst from solution of methanol with different nanocomposites those were ZnO/TiO_2, SnO/TiO_2, CuO/TiO_2, Al_2O_3/TiO_2 and CuO/Al_2O_3/TiO_2. It was found that CuO/Al_2O_3/TiO_2 Nano composite was most favorable for formation of hydrogen. Hydrogen production through photocatalytic activity was almost 10 times more than pure TiO_2 by using 0.2 wt. %CuO and 0.3 wt. % Al_2O_3/TiO_2. This Nano-sized photocatalyst has advantage of being inexpensive and environmentally benign H_2 production.

Yan Jian-Hui et al[96] presented Nitrogen doped $SrTiO_3/TiO_2$ composite photocatalysts for hydrogen production. Firstly, nitrogen doped $SrTiO_3$ was synthesized through solid phase method then merge with TiO_2 through sol-gel method then through hydrogen reduction process Pt-loaded composite were synthesized. Different techniques like XRD, UV-vis spectra; SEM and FT-IT were used for characterization purposes. Single $SrTiO_3$ and TiO_2 do not take part in hydrogen production. But their composite greatly enhanced photocatalytic hydrogen production. Optimized photocatalytic hydrogen production was achieved at 400 ℃ calcination temperature. Similarly, deposition of Pt also enhanced photocatalytic action and rate of average hydrogen production upto 5.1 mmol g cat-1h-1 with amount of 2 wt. % loaded Pt.

Perez-Larios et al[97] prepared TiO_2–ZnO mixed oxides and utilize it for production of hydrogen through water splitting. All mixed oxides have high surface area. These mixed oxides proved to be six times more efficient and active photocatalysts than bare TiO_2 semiconductor.

1.13 Synthesis of Nanomaterials

There are two main approaches for the synthesis of nanoparticles *i.e.*

    A. Top-down

    B. Bottom up

Top-down involves cutting of bulk matter to nanosized materials.

It includes:

- **Mechanical methods:** Grinding, slicing and ball mailing.
- **Lithographic methods**

Bottom up approaches involves assembly of materials to form desired products.

It includes:

Physical methods: sputtering, laser ablation and evaporation

Chemical methods:

- Sonochemical method
- Sol-gel method
- Hydrothermal method
- Co-precipitation method
- Micro emulsion method

1.13.1 Hydrothermal Synthesis of Nanoparticles

Since last fifteen years the hydrothermal method has been the most mainstream one, gathering enthusiasm from researchers and technologists of various disciplines. Word hydro means "water" and thermal means "heat". Sir Roderick Murchison (1792–1871) was the first one to use to explain the activity of water at high temperature and pressure[98].

In 1985 Rabenau gave definition of hydrothermal process as heterogeneous reactions in water solvent with temperature more than 100 °C and pressure 1 bar[99].

As per Roy hydrothermal process includes water as a catalyst and sometimes as a part of solid phases in the process at high temperature (>100 °C) and pressure (more than a few bar)[100].

Using water as solvent in hydrothermal processes has many advantages like:

- It is inexpensive.
- Environmental friendly.

- Behave as catalyst for synthesis of desired products by adjusting temperature and pressure.
- Nontoxic.
- Thermodynamically stable.
- Noncombustible.
- Non-carcinogenic.
- Removal of water is very easy as it is volatile.

1.13.2 Advantages of Hydrothermal Synthesis

(1): The expenses for apparatus, energy and precursors are quite less for hydrothermal technique.

(2): Hydrothermal techniques are more environmental friendly than many other methods, much different morphology and sizes of particles can be achieved by hydrothermal synthesis.

(3): Materials prepared through hydrothermal process frequently display contrasts in point defects when analyzed toward materials synthesized by elevated temperature preparation techniques. For example, materials like Tungstates of Ca, Ba, and Sr prepared at room temperature through hydrothermal technique don't have Schottky defects typically appears in similar materials synthesized at elevated temperatures which brings about enhanced luminescent properties.

(4): Hydrothermal synthesis can be combined with many other techniques like ultrasound, microwave, electro chemistry and optical radiation to get merits *e.g.* increase in reaction kinetics, and capability of making new materials.

(5): It does not require any surfactant or seed catalyst so it is very useful technique for large scale and cost effective production with good quality products.

Autoclave

A reaction vessel in which crystals grows under hydrothermal conditions is called "autoclave". In hydrothermal method, mostly very corrosive salts are being used to prepare inorganic substances for longer reaction time. So, the Autoclave must be able to withstand these corrosive solvents at elevated temperature and pressure for a longer time. The most successful corrosion resistant substance high-strength alloys, for example stainless steel, cobalt- based alloys, Fe, nickel, and Ti and its alloys. In order to avoid corrosion its material is coated with Teflon from inside as it is non-reactive. An ideal autoclave must be:

- Non-reactive towards acid, bases and oxidants.
- Easy to operate.
- Leak proof at high temperature and pressure.
- Capable of bearing high temperature and pressure for longer time duration.

Figure 1.5: Schematic illustration of autoclave

1.14 Objectives
The present work has following main objectives:

- To synthesize ZnO, ZnSe and ZnO/ZnSe heterostrucure through one-pot hydrothermal method.
- To analyze different characterizations of as synthesized photocatalysts using different techniques *e.g.*

1. XRD
2. SEM
3. TEM
4. EDS
5. UV-vis spectroscopy

- To examine photocatalytic application of as-synthesized products for the degradation of dye.

Chapter No. 2: Experimental and Characterization Techniques

2.1 Experimental

The experimental work involves the synthesis of ZnO/ZnSe common-cation heterostructure photocatalysts via one-pot hydrothermal method.

2.1.1 Chemicals

The chemicals used for the synthesis of the ZnSe/ZnO common-cation heterostructures are listed in Table 2.1 and were used without further purification. In addition, deionized water was used for the preparation of all the solutions.

Table 2.1: List of chemicals used for the synthesis of photocatalysts.

Serial No.	Chemical Name	Chemical formula	Molar mass (g/mol)	Percentage purity %	Company
1	Potassium Hydroxide	KOH	56.106	85-100	Sigma Aldrich
2	Zinc Acetate	$Zn(CH_3CCOO)_2$	219.50	99-102	Riedel-de Haen
3	Selenium powder	Se	78.96	99.5	Merck
4	Hydrazine Hydrate	N_2H_4	32.05	80 % in water	Merck

2.1.2 Hydrothermal Synthesis of ZnSe/ZnO Heterostructure Photocatalysts

A hydrothermal process was employed for the synthesis of ZnO/ZnSe heterostructure by using zinc acetate and se powder as precursor. In a typical synthesis approach, 0.175 g

(0.1 M) of zinc acetate and 0.0631 g (0.1 M) of se powder were added to 8 mL of 1 M KOH solution. Subsequently added 2 mL of hydrazine hydrate to above solution, then mixture was referred for constant stirring on magnetic hot plate for 1 hour at ambient temperature. The mixture was then transferred to 50 mL Teflon lined Autoclave. The autoclave was kept in heating oven at 200 ºC for 3 hours. Later on, the autoclave was cooled down to normal room temperature. The obtained yellow precipitates were collected and then washed with deionized water for several times and finally with ethanol. Then precipitates were dried at 70 °C in heating oven overnight. Dried ZnSe sample was ground and subjected to further analysis and characterization. Same procedure was repeated for different concentration of Se powder i.e. 0.075M, 0.05M, 0.025, 0.0M, while keeping all the reaction parameters (listed in Table 2.2) same as mentioned before and named them as NC1, NC2, NC3 & ZnO, respectively.

Table 2.2: Details of reaction parameters.

Sample ID	KOH conc. (M)	Time (h)	Zinc acetate (M)	Selenium conc. (M)	Temperature (◦C)
ZnSe	1	3	0.1	0.1	200
NC 1	1	3	0.1	0.075	200
NC 2	1	3	0.1	0.05	200
NC 3	1	3	0.1	0.025	200
ZnO	1	3	0.1	0.0	200

2.2 Characterization

The crystal structure and the phase of ZnO/ZnSe heterostructures were determined by X-Ray diffraction. XRD patterns have been recorded with CuKα radiations over the 2θ scale of 20 to 80º and the diffractometer used for this purpose was Bruker D8 focus with Ni-

filtered Cu-Ka radiation. Morphology and compositional analysis have been performed by using HITACHI S4800 Scanning electron microscopy (SEM) and for further detailed morphological studies HITACHI H-7700 transmission electron microscope (TEM) has been used. To obtain absorption spectra and to study optical properties of as-synthesized products for band gap calculation UV-vis spectrophotometer was used (lambda 750) with $BaSO_4$ as reference in range of 300 to 800 nm. Elemental composition in synthesized photocatalysts confirmed through energy dispersive x-ray spectroscopy analysis (EDS).

2.3 Characterization Techniques and their Basic Principles

Characterization techniques used for analyzing the properties of the given sample were as follow:

- X-ray Diffraction Crystallography (XRD)
- Energy Dispersive X-ray Spectrometry (EDX)
- Scanning Electron Microscopy (SEM)
- Transmission Electron Microscopy (TEM)
- UV-visible Spectroscopy

2.3.1 X-Ray Diffraction Crystallography (XRD)

XRD is a strategy which is utilized for the investigation of crystal materials. Important parts of diffractometer include X-ray tube, goniometer, sample holder, incidents and receiving optics and detector.

It gives data about crystalline materials (surface, crystallinity, dimensions, phase purity defects and so forth). Different diffraction peaks show up because of interaction of monochromatic X-Ray light with the planes of crystalline materials. This peak pattern is for every material. Furthermore, internationally information base is given to identify crystalline specimens i.e. ICDD (International Centre for Diffraction Data). Optical modules are also attached with the XRD, based on analysis required it can be changed

keeping the accuracy of position unchanged. High resolution XRD can be achieved simply by exchanging line and point focus of X-ray beam. Analysis can be more diverse by using different optical modules i.e. thin films, fabricated parts, powders and epitaxial film can easily be analyzed [101].
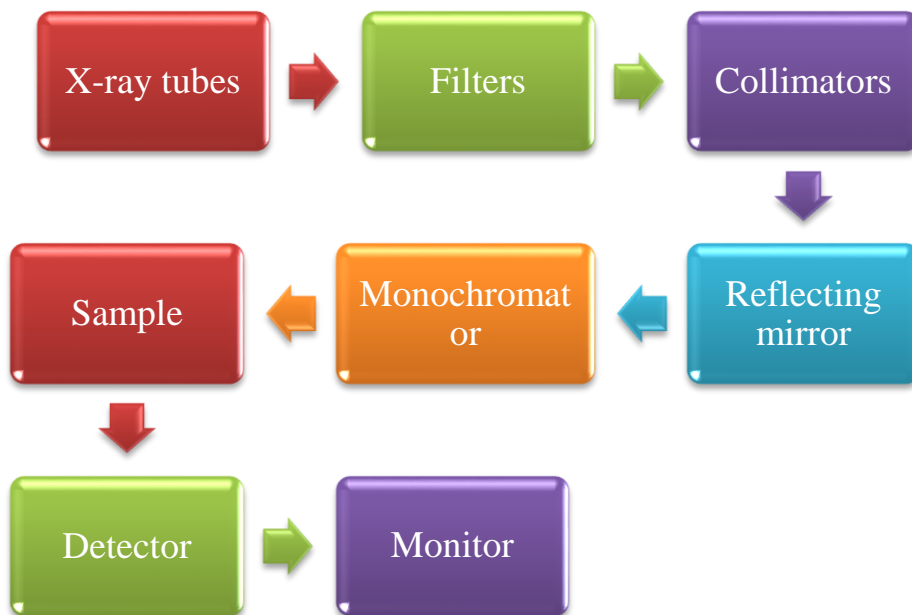
Figure 2.1: Flow chart shows different parts of X-ray diffractometer.

2.3.1.1 Basic Principle of XRD

When electron of sufficient energy strikes and removes electrons of inner shells of the material, specific X-ray spectra is formed. To measure the intensity of reflected X-rays detectors are attached with the XRD. When characteristics of incidents X-ray striking, the sample satisfies the Bragg's equation then peak intensity appears due to constructive interference. Then detector after recording the X-rays change the signal to the count rate and then it is exhibited in the computer. Sample rotates at the angle of θ in the way of X-ray beam while detectors which in placed to record the signals rotates at the angle of 2θ [102].

2.3.1.2 Applications

- Phase purity
- Crystallite size determination

$$D = \frac{K\lambda}{\beta Cos\theta}$$

[Where, D= crystallite size, K= shape factor, λ= wavelength, β= full width half maxima, θ = Bragg's angle]

- Measure the crystallinity of sample
- Compositional analysis

By using other specialized techniques with XRD can be used for

- Identification of crystal structure
- Quantify different compounds
- Analysis of thin films
- Surface analysis like direction of particles

2.3.1.3 Strength

- Rapid and non-destructive technique for structure identification
- Small amount of sample is required
- Data interpretation is relatively easy

2.3.1.4 Limitations

- Must require access to reference data file
- Sample must be grinded into fine powders
- Detection limit is ~ 2 % of specimen for more than 2 materials.
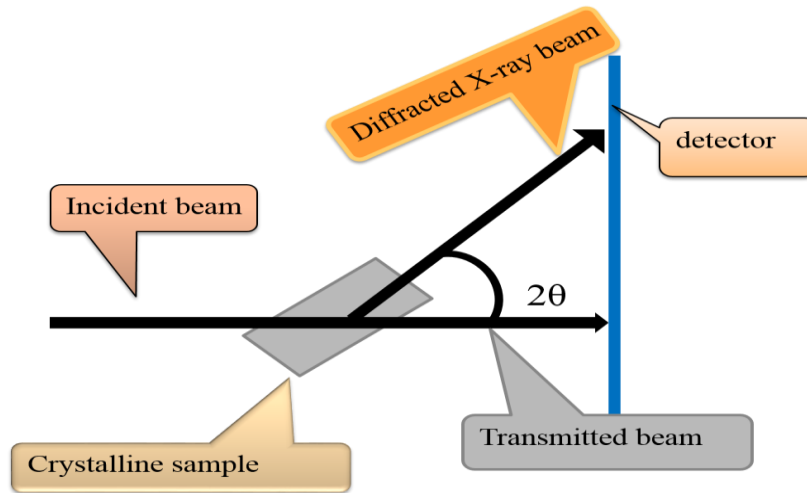
Figure 2.2: Typical layout of diffractometer.

2.3.2 Scanning Electron Microscopy (SEM)

Scanning Electron Microscopy provides high resolution three-dimensional image of the specimen, by interacting a focused electron beam with the sample under investigation. This technique is very valuable for studying the surface of the sample.

SEM basically comprises of following components already illustrated in(Fig 2.3),

a) Electron column
b) Scanning system
c) Detection system
d) Visible display
e) Vacuum system and
f) Electronic control system

SEM images are produced by using a fine probe for the interaction of electron beam across the surface of sample. For this purpose, scanning coils are used along with probe for proper focusing and scanning. An electromagnetic radiation is emitted through each point on the

surface that is interacting with the electron beam. Signal is collected on the detector that is due to the secondary electrons and back scattered electrons from that specific portion of the electromagnetic radiation and shown on a TV screen or PC screen. The subsequent picture is for the most part clear to translate, in any event for topographic information of items at low amplifications (Fig. 2.3)[103, 104].
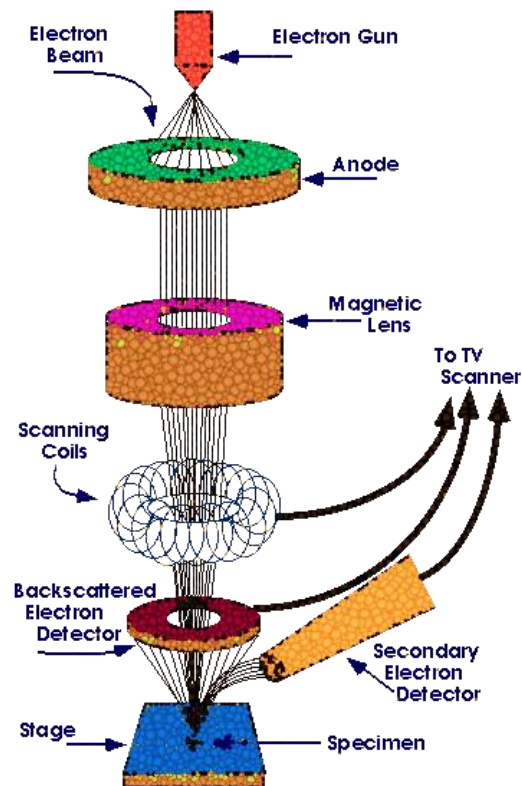
Figure 2.3: Layout of major components of SEM.

2.3.2.1 Applications

SEM has numerous applications including:[105]

- Gives information regarding composition and morphology

- Provide qualitative analysis and determine crystalline structure
- Provides the particle size
- Microchip assembly for computers
- Semiconductors analysis
- Many biological applications

2.3.2.2 Advantages

- Very small quantity of sample is enough
- Very quick technique
- Sample can be analyzed in 3D image
- No specific thickness of sample is required

2.3.2.3 Disadvantages

- Costly
- Risk of exposure to radiation as electrons released below the sample.
- Limited to solids sample only and that can handle average vacuum pressure as well.
- Sample must be conductive.
- Resolution in SEM is less than TEM.

2.3.3 Transmission Electron Microscopy (TEM)

TEM consist of following components,

- Source of electron
- 2 condensers
- Sample port
- lenses

- Vacuum chamber

- Fluorescent screen

- Computer
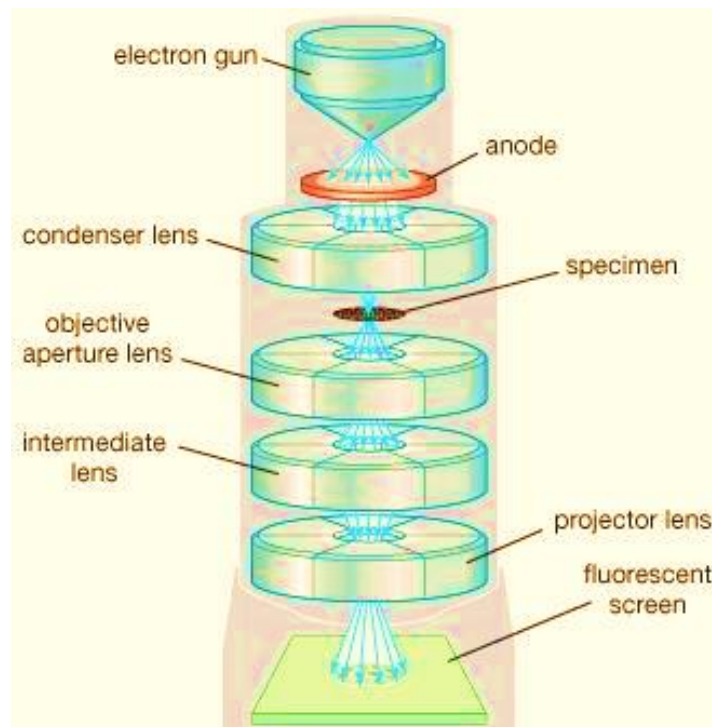
Figure 2.4: Layout of major components of TEM.

2.3.3.1 Basic Principle

In this technique beam of electron is passed through ultra-thin sample. Electrons are used instead of photons and instead of glass lenses electromagnetic lenses used and image viewed on screen these entire characteristics make TEM more efficient and better than ordinary microscope. Interaction of crystalline specimen with the beam of light is by diffraction instead of absorption. The power of the diffraction relies upon the direction of the planes of elements in crystal structure with respect to the electron beam. A high contrasting picture can be shaped by stopping electrons which are deflected results in

variety of intensities of electron that uncovers data of crystalline structure. It will generate bright and dark field images. Light portion represents large number of electrons passed through the specimen while dark portion reflects dense portion of sample. (Fig. 2.4)[106, 107].

2.3.3.2 Applications

- It gives surface, morphology and composition of crystalline structure
- Semiconductor analysis also used in silicon chips and PC manufacturing
- Nano sized particles can be studied in detail and depth

2.3.3.3 Advantages

- Very good resolution almost 1000 times more than ordinary microscope.
- Sample can be analyzed in depth and detain with TEM
- Images obtained from TEM are of very good quality and detailed.
- Position of atom can also be determined

2.3.3.4 Disadvantages

- Very thin layer should be used
- Expensive and time taking
- Images only appear in black and white.
- It gives 2D image
- Magnification is up to 50 million
- Difficult and specific sample preparation
- TEM requires special maintenance
- Cannot be used on living organisms.

2.3.4 UV-visible Spectroscopy

This technique determines the analyte concentration by using light absorption by analyte at specific wavelength. It is also called Electronic spectroscopy as it involves the transition of electron from ground start to excited state. It follows Beer-Lambert's law which states that when monochromatic light transfer through mixture of absorbing material, with the thickness of mixture rate of reduction of radiation intensity is directly related to incident beam and concentration of mixture[108].

Beer-Lambert's law is as follow:

A=$A = log I_\circ /$I= εcl

(Where, ε = molar absorptivity, l = path length of light, $I_\circ$= intensity of incident beam, I = intensity if reflected beam)

From Beer-Lambert's law, it is evident that Increasing the number of absorbing molecules will increase the extent of light absorption.

Instrumentation includes:

- Source of light
- Monochromator
- Sample holder and reference cell
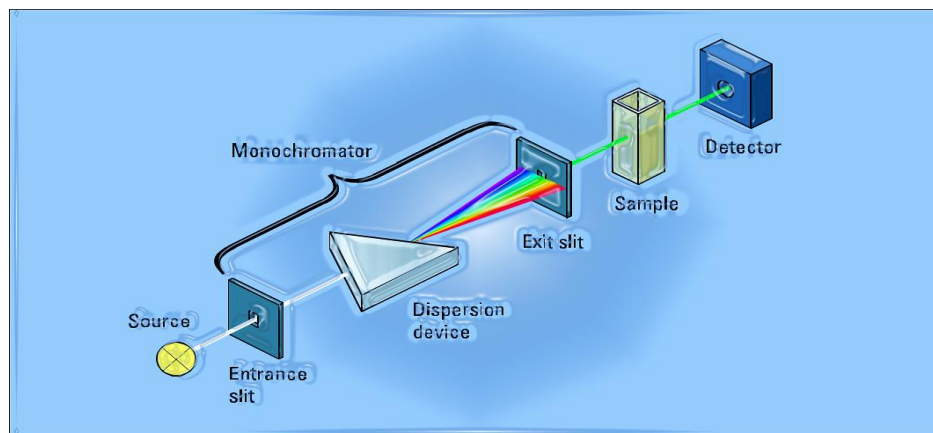- Detector
- Amplifier
- Monitor

Figure 2.6: Block diagrammatic representation of UV-spectrophotometer.

2.3.4.1 Applications
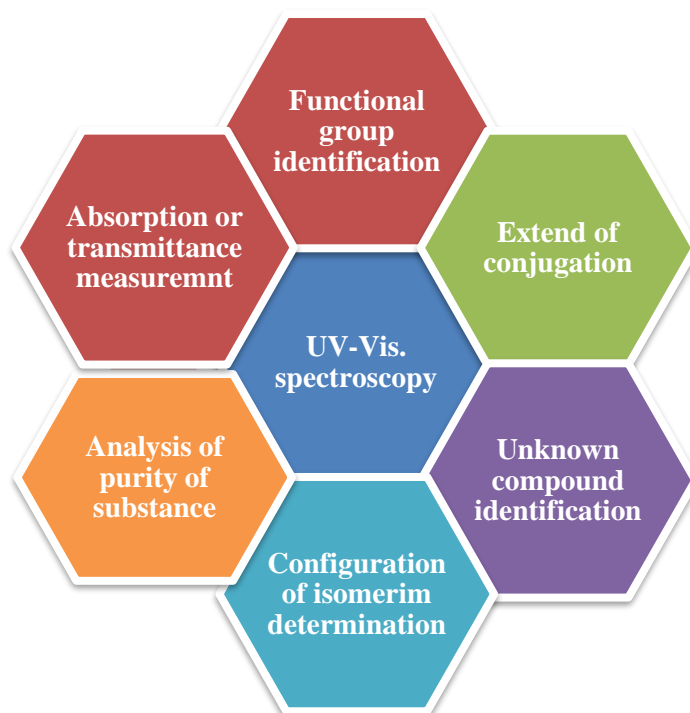
UV finds its applications in [109] :

Figure 2.5: Applications of UV-Visible spectroscopy

2.3.4.2 Advantages

- Highly sensitive
- Less sample quantity required
- Linear response over large concentration ranges
- Simple construction and cost effective

2.3.4.3 Disadvantages

- Only work for compound which absorb light
- Less accurate

2.3.5 Energy Dispersive X-ray Spectroscopy

EDS consist of following components

- X-ray beam source
- Pulse processor
- Detector
- Analyzer

The EDS procedure identifies x-beams radiated from the specimen when an electron beam strikes to describe the composition of elements of desired volume. At the point when SEM electrons strike the specimen, electrons are released out from the element comprising the specimen's surface. The subsequent electron holes are filled by electrons from a higher state, and thus x-ray-beam is transmitted to adjust the difference of energy between the higher and lower electronic states. The x-beam energy is representative of the element from which it was discharged. The detector evaluates the relative abundance versus energy of x-ray beam it produces the charge pulse directly related to x-ray energy when electrons are bombarded. Then with the help of amplifier the charge pulse it changed to voltage

pulse and signal is transferred to the analyzer which analyzes the energy of each pulse through voltage and sends the data to computer monitor. Energy versus counts spectrum of x-rays is analyzed in order to fine elemental composition of samples (Fig.2.7)[110].
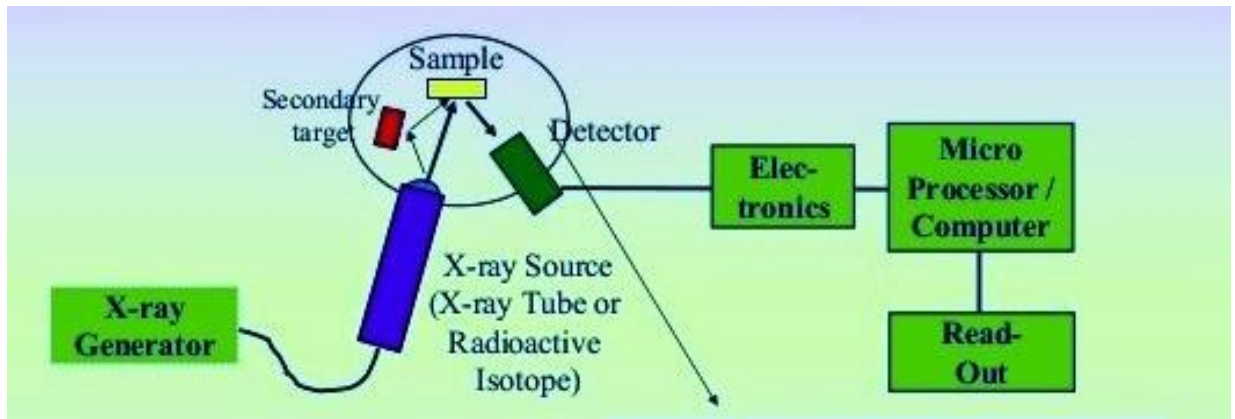

Figure 2.7: Energy Dispersive X-ray Spectrometer.

2.3.5.1 Applications

EDX is most used for [111]:

- Elemental analysis,
- corrosion identification,
- external material analysis,
- percentage composition
- defect identification

2.3.5.2 Advantages

- Gives elemental analysis
- Quick identification of contaminations
- Cost effective
- Easily available

- Gives quantitative analysis for some samples

2.3.5.3 Disadvantages

- Sometimes peak overlapping occurs make analysis difficult
- Normally semi-quantitative analysis is possible with EDX
- Vacuum compatibility for sample is necessary so not suitable for wet organic compounds
- Microphonic

2.4 Photocatalytic Activity

Photocatalytic activities of the ZnO, ZnSe and ZnO/ZnSe composite were examined for the degradation of Congo red under UV-vis. irradiation. λ_{max} value of dye was calculated by using UV-vis spectrophotometer. Source of light used for the degradation process was 300 W Xe arc lamp which was placed at 15 cm distance over 250 mL vessel having 75 ppm of Congo red in dark. One control experiment was carried out in the absence of catalyst no degradation was observed during this period. Congo red was found to be very stable dye under light irradiation but in the absence of photocatalyst.

Then to ensure adsorption-desorption equilibrium between dye solution and photocatalyst, 100 mg of catalyst was added in 100 mg of Congo red solution in dark with constant 10 min stirring. After every 5 minutes of light irradiation 5 mL solution was taken for degradation analysis. λ_{max} was measured by measuring concentration of samples with respect to time photocatalytic activity was evaluated by UV-vis. spectrophometer.

Chapter No. 3: Results and Discussion

3.1 Phase Analysis
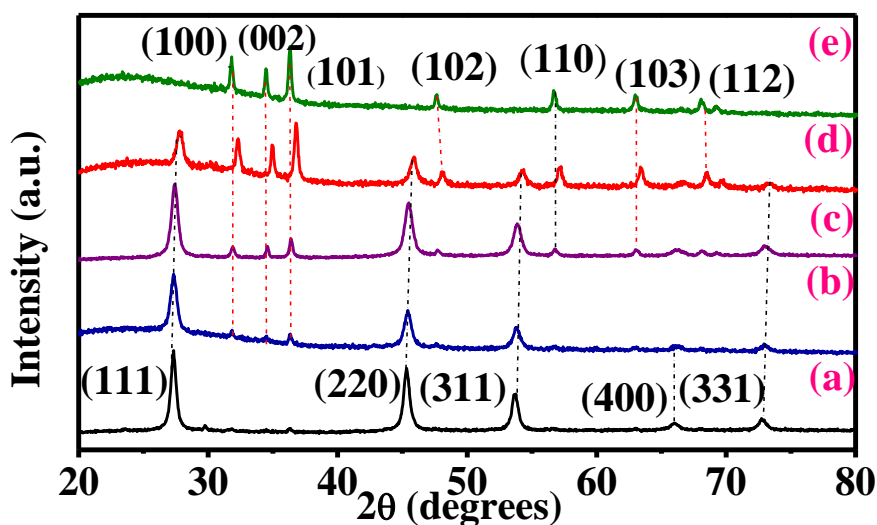
Figure 3.1: (XRD) patterns of (a) ZnSe, (b-d) ZnO–ZnSe heterostructures with 75%, 50% and 25% ZnSe (e) ZnO.

The crystal structure and purity of the synthesized photocatalysts was confirmed through the X-ray powder diffraction in the 2θ range of 20 to 80° and the results are shown in the Figure 3.1. In case of ZnSe (Fig. 3.1a), peaks were in full agreement with the available standard JCPDS (Joint Committee on Powder Diffraction Standards) number 00-037-1463 where all peaks confirmed its cubic structure with estimated lattice constant of 0.5668 nm. All these lattice parameters were consistent with already reported standards. While in case of ZnO (Fig. 3.1e), it was observed to be phase pure as per the available standard diffraction patterns (JCPDS no. 00-036-1451). Where whole diffraction pattern confirms the synthesis of hexagonal wurtzite ZnO with estimated lattice parameters of a = 0.3249

nm and c = 0.5206 nm. In addition, for the ZnSe/ZnO heterostructure (Fig. 3.1b-d), all the peaks were matched either from ZnSe and/or from ZnO in Fig. 3.1, and there was no extra peak present in the composite which also confirms the successful formation of the heterostructure photocatalysts. Furthermore, moving from (a) to (e) in Fig. 3.1, intensity of peaks decreases but width increases which means crystallinity decreases and crystallite size increases which is calculated using scherrer equation (1) *i.e.* 39 nm for ZnSe while crystallite size of ZnO is 79 nm. Similarly, cell volume of ZnSe and ZnO was calculated using (2) and (3) formulas respectively. All the values are listed in Table 3.1.

$$D = \frac{k\lambda}{\beta \cos \theta} \qquad (1)$$

Where,

D = crystallite size

K = shape constant i.e. 0.89

λ = wavelength of X-ray radiation

β = full width at half maxima (FWHM)

θ = diffraction angle

Cell volume

V= a^3 (for cubic system) $\qquad$ (2)

V= 0.866 a^2c (for hexagonal system) $\qquad$ (3)

Table 3.1: Crystalline parameters calculated from XRD patterns for ZnO and ZnSe.

(hkl)		Crystallite Size (nm)	Average Crystallite Size (nm)	Cell Volume ($\mathring{A}^3$)	Lattice constants ($\mathring{A}$)
ZnO	**(100)**	71.9	79	47.62	a = b= 3.2498
	(002)	101.4			
	(101)	72.7			
	(102)	59.1			
	(110)	180.5			c = 5.2066
	(103)	38.0			
	(112)	30.9			
ZnSe	**(111)**	33.4	39	182.17	a=b=c= 5.6688
	(220)	39.3			
	(311)	77.4			
	(400)	21.5			
	(331)	25			

3.2 Elemental Analysis

Compositional and stoichiometric analysis has been done by using energy dispersive X-ray spectroscopy (EDX). Analysis showed that in sample (a) there were only 2 elements *i.e.* Zn, Se were present which confirmed synthesis of ZnSe (Fig 3.2a). Fig 3.2b-d indicated presence of Zn, O and Se which confirmed the formation of heterostructures ZnO/ZnSe. Moving from Fig 3.2b to 6d it is evident that peak intensity of Se continuously decreases while that of Oxygen increases which confirmed that quantity of ZnO increases and ZnSe decreases and in Fig 3.2e only peaks of Zn and O were observed which confirmed only ZnO formation.
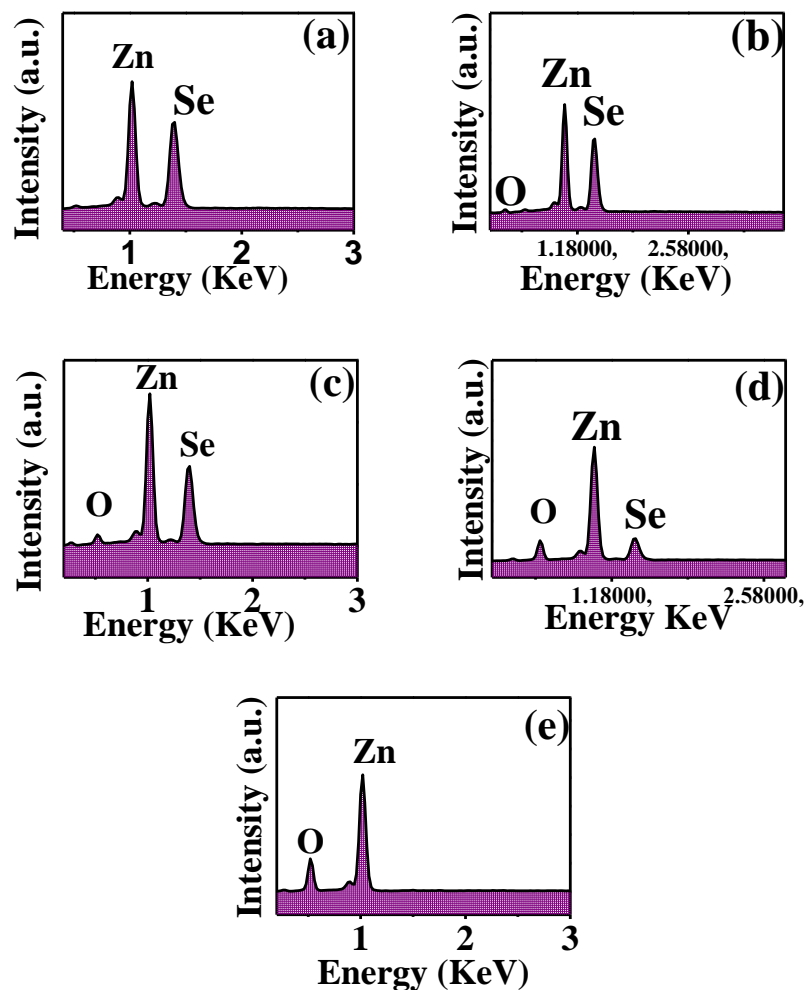
Figure 3.2: EDX spectra of (a)ZnSe, (b-d) ZnO/ZnSe heterostructures with 75%, 50% and 25% ZnSe and (e) ZnO.

3.3 Morphological Analysis

SEM analysis was carried out to confirm the morphology of the synthesized photocatalysts and the results are presented in Fig. 3.3 it is apparent from the Fig. 3.3(a) that ZnSe particles are spherical in shape and are in agglomerated form. On the other hand, ZnO has grown in rod-like structures which can clearly be observed in Fig. 3.3(e). However, both spherical ZnSe as well as rod-like ZnO nanostructures can clearly be seen in case of

ZnO/ZnSe heterostructure (Fig. 3.3b-d) which might also facilitate the formation of interface to facilitate the photo generated charge separation for the efficient photocatalytic Congo red dye degradation. Furthermore, dimensions of the samples were calculated using SEM analysis *i.e.* spherical ZnSe have particle size in the range of 20 nm to 50 nm which agrees with crystallite sizes calculated from XRD data. While rod like ZnO has thickness nearly 50 nm-100 nm and length ranges from 150 nm-400 nm as given in Table 3.2.

Figure 3.3: SEM images of ZnSe/ZnO heterostructures with different amount of ZnSe: (a) 100% (*i.e.,* pure ZnSe), (b) 75% (c) 50% (d) 25 % and (e) 0% (*i.e.*, pure ZnO).

Table 3.2: Dimensions of ZnO and ZnSe from SEM.

Sample Type	Dimensions (nm)
ZnO	Thickness ~ 50-100 Length ~ 150-400
ZnSe	~ 20- 50

For further closer morphological analysis, structures were examined by TEM and results are displayed in Fig 3.4. In TEM image for pure ZnSe (Fig. 3.4 a) spherical nanoparticles can be seen clearly. Nanocomposite with 25% ZnO (Fig. 3.4 b) nanorods of ZnO starts diffusing with spherical ZnSe nanoparticles. In Fig 4c and 4d close connection between both ZnSe spheres and ZnO rods is clearly observable and as the amount of ZnO is increasing in composite its particles start depositing on the surface of ZnSe Nano spheres which confirmed the formation of heterostructures. Results obtained from TEM are in agreement with results of SEM and XRD.
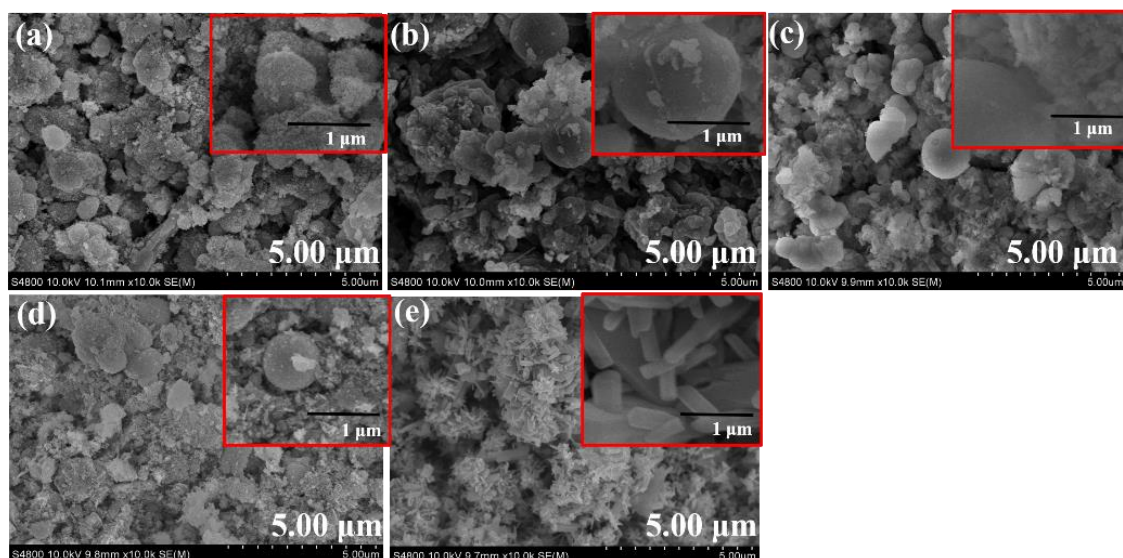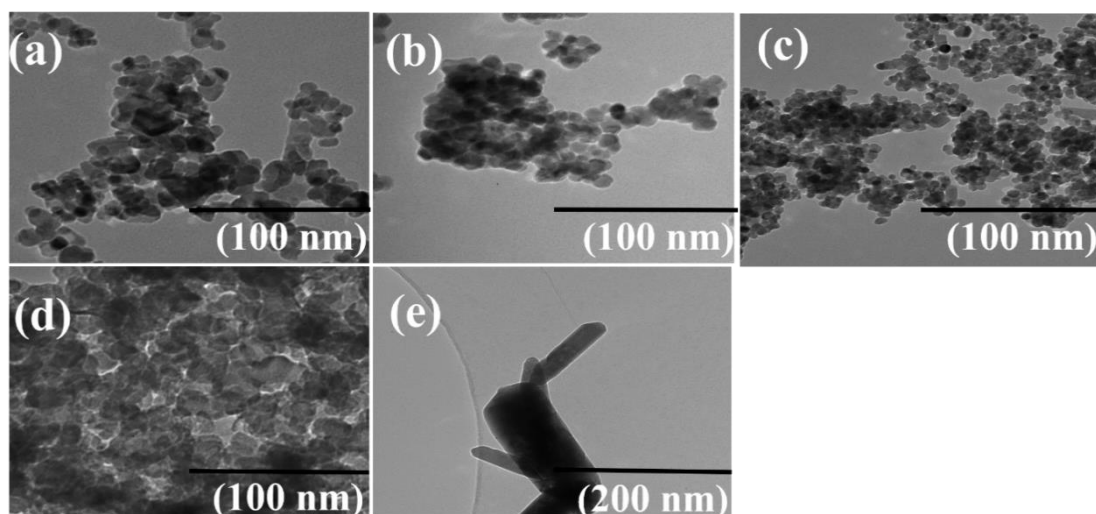

Figure 3.4: TEM images of ZnSe/ZnO heterostructures with different amount of ZnSe: (a) 100% (*i.e.,* pure ZnSe), (b) 75% (c) 50% (d) 25 % and (e) 0% (*i.e.*, pure ZnO).

3.4 UV-Vis Spectroscopy

UV-visible diffuse reflectance spectroscopy was then employed to investigate the optical properties of the synthesized photocatalysts and the results are shown in the Figure 3.5. As represented in Fig. 3.5(a), ZnO shows a strong absorption edge at ~ 385 nm corresponding to its energy bandgap of 3.2 eV calculated via Tauc plot as shown in the

inset. On the other hand, ZnSe shows a sharp absorption peak at ~ 490 nm with the bandgap energy of 2.64 eV as shown in the Fig. 3.5(b).
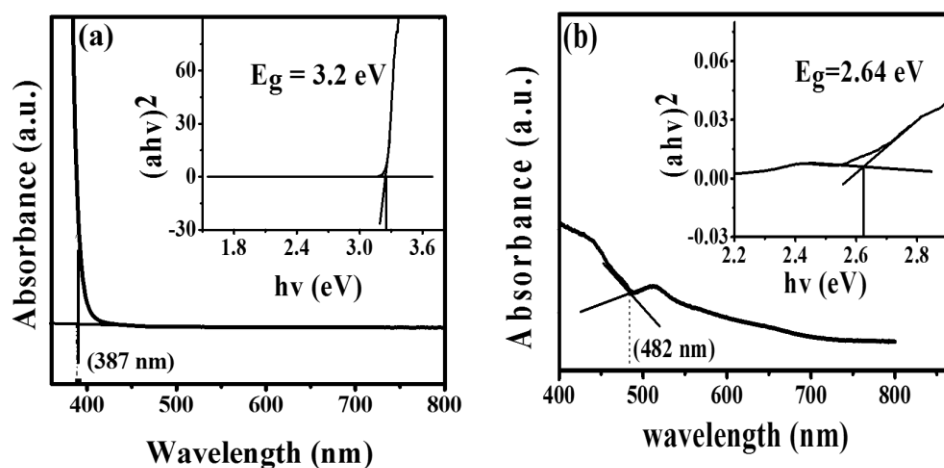
Figure 3.5: UV-vis spectra and Tauc plots (insets) for (a) ZnO, and (b) ZnSe.

3.5 Alignment of energy levels

The alignment of energy levels is an important parameter to study the degradation pathway in photocatalytic reaction systems. Based on the results obtained from UV-vis diffuse reflectance spectroscopy as well as the valence band positions of constituent photocatalysts available from the literature,[112, 113] the alignment of energy levels of ZnO/ZnSe heterostructure photocatalyst is hereby presented in the Fig. 3.6.
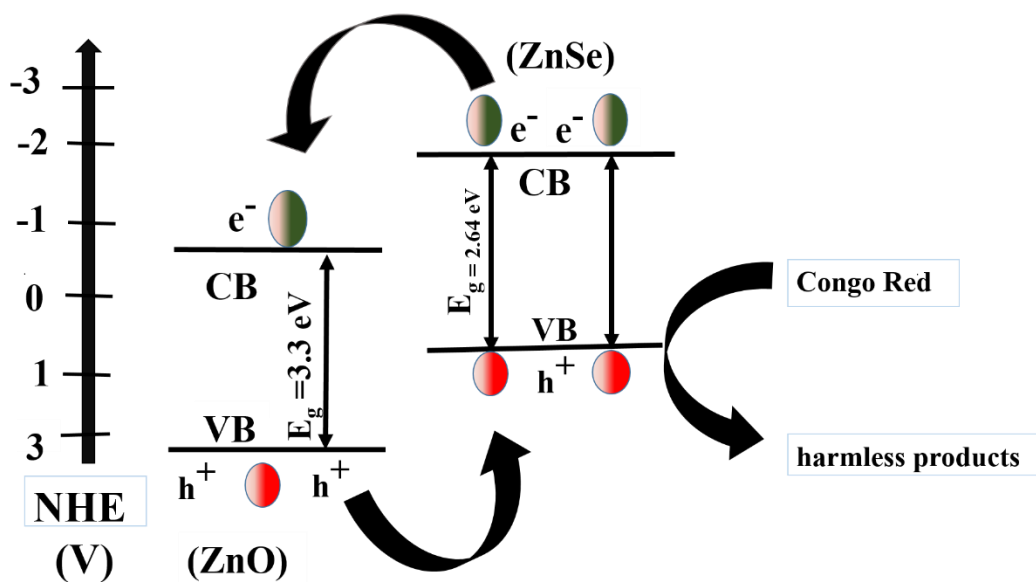
Figure 3.6: Alignment of energy levels for ZnO/ZnSe heterostructure photocatalyst

3.6 Photocatalytic Activity

Finally, the as-synthesized photocatalysts have been used for the photocatalytic degradation of Congo red dye under the UV-visible light irradiation and the results are shown in the Fig. 3.7 a graph between degradation percentage and time. Degradation efficiency of Congo red was measured using following formula:

$$DE = \frac{C_0 - C_t}{C_0} * 100 \quad (4)$$

Where, C_o is initial concentration of Congo red white C_t is dye concentration after time t. results showed that after 40 minutes of light irradiation about 91% of Congo red molecules degraded using ZnO/ZnSe nanocomposite.

On the other hand, bare ZnO and ZnSe, the degradation efficiency is comparatively lower than the heterostructure photocatalyst which is attributed to the rapid electron-hole recombination in these bare constituents which ultimately result in the poor efficiency.

56

The ZnO/ZnSe composite has shown the best results which is due to the efficient charge separation and the results can be explained based on the alignment of energy levels. As shown in Fig. 3.6, the heterostructure is irradiated with UV-visible light; it results in the excitation of electrons into the conduction bands in both ZnO as well as ZnSe semiconductors thereby leaving the holes behind it their valence bands (eqn. 5). Attributed to the suitable positions of conduction band minimum (CBM) and valence band maximum (VBM), the electrons from the conduction band of ZnSe are transferred to the conduction band of ZnO (eqn. 6), and the holes from ZnO valence band are thus transferred to the valence band of ZnSe (eqn. 7), thereby minimizing the charge recombination. The electron on ZnO reacts with dissolved oxygen to form superoxide radical anions ($O_2^{\cdot-}$) (eqn. 8). This($O_2^{\cdot-}$) is very reactive specie it generates hydroxyl radicals ($HO^{\cdot}$) On reaction with water (eqn 9), then electron upon interacting with H_2O_2 also produce hydroxyl radicals (eqn. 10). Meanwhile, holes are caught by the hydroxyl ions or water molecules at catalyst surface to form hydroxyl radicals ($HO^{\cdot}$) (eqn. 11,12) which plays very important part in dyes degradation. Superoxide radical anion on reaction with proton gives hydroperoxy radical HO_2 (another very reactive specie) (eqn. 13). Already reported literature suggested that benzene and naphthalene derivatives formed as intermediate products during Congo red degradation (eqn. 14) which on further reaction with hydroxyl radicals gives CO_2 and H_2O (eqn. 15). The possible photocatalytic mechanism exhibited by as synthesized heterostructure has been presented as follows[69]:

$$photocatalyst + h\upsilon \rightarrow photocatalyst\ (e^- + h^+) \tag{5}$$

$$ZnSe(e^-) + ZnO \rightarrow ZnSe + ZnO\ (e^-) \tag{6}$$

$$ZnO(h^+) + ZnSe \rightarrow ZnSe(h^+) + ZnO \tag{7}$$

$$ZnO\ (e^-) + O_2 \rightarrow ZnO + O_2^{\cdot-} \tag{8}$$

$$O_2^{\cdot-} + H_2O \rightarrow H_2O_2 + HO^{\cdot} + OH^- \tag{9}$$

$$H_2O_2 + ZnO(e^-) \rightarrow ZnO + OH^- + HO^\cdot \tag{10}$$

$$ZnSe(h^+) + OH^- \rightarrow ZnSe + HO^\cdot \tag{11}$$

$$ZnSe(h^+) + H_2O \rightarrow ZnSe + HO^\cdot + H^+ \tag{12}$$

$$O_2^{\cdot-} + H^+ \rightarrow HO_2^\cdot \tag{13}$$

$$HO_2^\cdot + O_2^- + HO^\cdot + Cong\ red \rightarrow Naphthalene\ derivatives\ + di-$$
$$substituted\ benzene\ derivatives \tag{14}$$

$$HO^\cdot + naphthalene/benzene\ derivatives \rightarrow CO_2 + H_2O \tag{15}$$
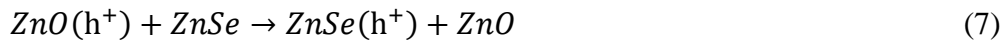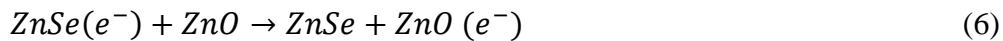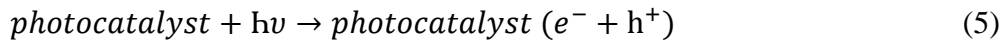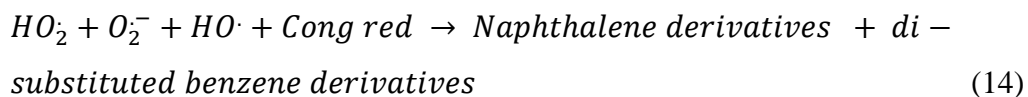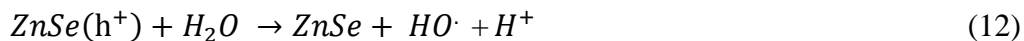
In addition, a control experiment was also performed under light but in the absence of photocatalyst, no dye degradation was observed during this period.
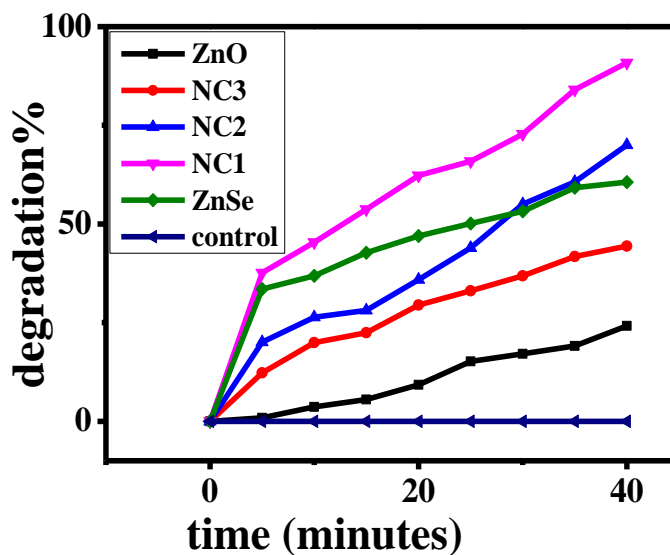
Figure 3.7: %age photocatalytic degradation of Congo red over synthesized photocatalysts under UV-visible irradiation.
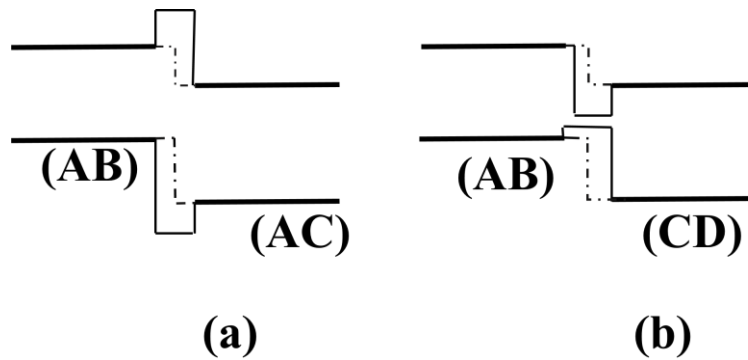
Figure 3.8: Expected band arrangement in heterojunction type II (a) with common cation and (b) without common cation

Moreover, presence of common cation in heterostructure greatly enhance the photocatalytic activity. Interface, with an energy gap greater than its component's band gap usually lessen the recombination of charge carriers and keep them in separate layer hence photocatalytic activity improved Fig. 3.8a. while heterostructures with no common cation or anion exhibit decreased photocatalytic activity as band gap of components is greater than interface with an energy gap results in electrons-holes recombination. Fig 3.8b.

Chapter No. 4: Summary and Outlook

We have synthesized ZnO/ZnSe heterostrured photocatalysts via hydrothermal route and utilized it for the efficient degradation of the di azo dye *i.e.* Congo red.

Main highlights of thesis work are given as below:

4.1 Highlights

- ZnO/ZnSe heterostructure successfully synthesized via one pot hydrothermal route.
- Synthesized photocatalysts were subjected to different techniques including XRD, SEM, TEM, EDX and UV-visible spectroscopy for phase analysis, morphological studies, elemental composition and to investigate optical properties.
- As-synthesized photocatalysts were then efficiently utilized for the degradation of Congo red dye under UV-Visible light irradiation.
- Formation of ZnO/ZnSe heterostructure increases the charge transfer between ZnSe to ZnO through close interface formation and thus decrease the electrons-holes recombination.
- Heterostructure with 75% ZnSe content exhibited the highest photocatalytic activity by degrading 90% of dye in 40 minute, as compared to its bare constituents *i.e.* ZnO and ZnSe. Which is attributed to the efficient charge separation and presence of common cation in heterostructure.

4.2 Future Perspectives

- Owing to the alignment of their energy levels in ZnO/ZnSe, similar photocatalytic systems can also be employed in the degradation of many other dyes, photovoltaic cells and water splitting for H_2 generation in future studies.

- In order to get enhanced photocatalytic applications further efficient techniques must be developed to suppress the recombination of photogenereted charge carriers.

- Prolonged exposure to light also cause deactivation of photocatalysts this issue needs to be address in future.

References

1. T. Tsoutsos, N. Frantzeskaki and V. Gekas, *Energy Policy*, 2005, **33**, 289-296.
2. M. K. Hill, *Understanding Environmental Pollution*, Cambridge University Press, 2010.
3. P. E. Stackelberg, E. T. Furlong, M. T. Meyer, S. D. Zaugg, A. K. Henderson and D. B. Reissman, *Science of the total environment*, 2004, **329**, 99-113.
4. D. Clifford, S. Subramonian and T. J. Sorg, *Environmental science & technology*, 1986, **20**, 1072-1080.
5. P. K. Goel, *Water Pollution: Causes, Effects and Control*, New Age International, 2006.
6. R. P. Schwarzenbach, T. Egli, T. B. Hofstetter, U. von Gunten and B. Wehrli, *Annual Review of Environment and Resources*, 2010, **35**, 109-136.
7. R. Kant, *Natural Science*, 2012, **04**, 22-26.
8. M. A. Brown and S. C. De Vito, *Critical reviews in environmental science and technology*, 1993, **23**, 249-324.
9. I. K. Konstantinou and T. A. Albanis, *Applied Catalysis B: Environmental*, 2004, **49**, 1-14.
10. V. Augugliaro, C. Baiocchi, A. B. Prevot, E. García-López, V. Loddo, S. Malato, G. Marcí, L. Palmisano, M. Pazzi and E. Pramauro, *Chemosphere*, 2002, **49**, 1223-1230.
11. B. de Campos Ventura-Camargo and M. A. Marin-Morales, *Textiles and Light Industrial Science and Technology*, 2013.
12. H. Zollinger, *Color chemistry: syntheses, properties, and applications of organic dyes and pigments*, John Wiley & Sons, 2003.
13. Z. Carmen and S. Daniela, Organic Pollutants Ten Years After the Stockholm Convention-Environmental and Analytical Update, 2012.
14. Y. H. Lee and S. G. Pavlostathis, *Water research*, 2004, **38**, 1838-1852.
15. F. Copaciu, O. Opriş, V. Coman, D. Ristoiu, Ü. Niinemets and L. Copolovici, *Water, Air, & Soil Pollution*, 2013, **224**, 1478.
16. R. W. Baker, *John Wiley & Sons, Ltd*, 2004, 96-103.
17. A. K. Verma, R. R. Dash and P. Bhunia, *Journal of environmental management*, 2012, **93**, 154-168.
18. A. M. Lotito, U. Fratino, G. Bergna and C. Di Iaconi, *Chemical Engineering Journal*, 2012, **195**, 261-269.
19. Z. Wang, M. Xue, K. Huang and Z. Liu, in *Advances in Treating Textile Effluent*, InTech, 2011.
20. F. Gaehr, F. Hermanutz and W. Oppermann, *Water Science and Technology*, 1994, **30**, 255-263.
21. L. Yang, G. Nakhla and A. Bassi, *J. Hazard. Mater.*, 2005, **125**, 130-140.

22. B. Kasprzyk-Hordern, M. Ziółek and J. Nawrocki, *Applied Catalysis B: Environmental*, 2003, **46**, 639-669.
23. H. Sontheimer, J. C. Crittenden and R. S. Summers, 1988.
24. Y. Kato, K. Kakimoto, H. Ogawa, M. Tomari, E. Sakamoto and T. Asahara, *Kogyo Yosui*, 1986, 37-45.
25. P. Janoš, S. Coskun, V. Pilařová and J. Rejnek, *Bioresour. Technol.*, 2009, **100**, 1450-1453.
26. C. A. Martinez-Huitle and S. Ferro, *Chem. Soc. Rev.*, 2006, **35**, 1324-1340.
27. O. Legrini, E. Oliveros and A. Braun, *Chem. Rev.*, 1993, **93**, 671-698.
28. F. Barbette, F. Rascalou, H. Chollet, J. Babouhot, F. Denat and R. Guilard, *Anal. Chim. Acta*, 2004, **502**, 179-187.
29. G. T. Daigger, J. R. Borberg and L. M. Morales, Google Patents, 1989.
30. E. Muller, A. Stouthamer, H. W. v. van Verseveld and D. Eikelboom, *Water Res.*, 1995, **29**, 1179-1189.
31. M. N. Chong, B. Jin, C. W. Chow and C. Saint, *Water Res.*, 2010, **44**, 2997-3027.
32. X. Chai, T. Kobayashi and N. Fujii, *Sep. Purif. Technol.*, 1999, **15**, 139-146.
33. R. Casa, A. D'Annibale, F. Pieruccetti, S. R. Stazi, G. G. Sermanni and B. L. Cascio, *Chemosphere*, 2003, **50**, 959-966.
34. J. Vymazal, *Ecol. Eng.*, 2005, **25**, 478-490.
35. Y.-C. Oh, 2004.
36. J. M. Coronado, F. Fresno, M. D. Hernández-Alonso and R. Portela, *Design of advanced photocatalytic materials for energy and environmental applications*, Springer, 2013.
37. A. Fujishima and K. Honda, *nature*, 1972, **238**, 37-38.
38. J.-M. Herrmann, *Catal. Today*, 1999, **53**, 115-129.
39. J. A. Rodriguez and M. Fernández-García, *Synthesis, properties, and applications of oxide nanomaterials*, John Wiley & Sons, 2007.
40. A. L. Linsebigler, G. Lu and J. T. Yates Jr, *Chem. Rev.*, 1995, **95**, 735-758.
41. D. Chatterjee and S. Dasgupta, *Journal of Photochemistry and Photobiology C: Photochemistry Reviews*, 2005, **6**, 186-205.
42. M. M. Khan, S. F. Adil and A. Al-Mayouf, Elsevier, 2015.
43. A. K. Arora, V. S. Jaswal, K. Singh and R. Singh, *Orient. J. Chem*, 2016, **32**, 2035-2042.
44. E. Pelizzetti and C. Minero, *Comments on Inorganic Chemistry*, 1994, **15**, 297-337.
45. K. Zhang and L. Guo, *Catalysis Science & Technology*, 2013, **3**, 1672.
46. C.-H. Lai, M.-Y. Lu and L.-J. Chen, *Journal of Materials Chemistry*, 2012, **22**, 19-30.
47. M. Ni, M. K. Leung, D. Y. Leung and K. Sumathy, *Renewable and Sustainable Energy Reviews*, 2007, **11**, 401-425.

48. A. Umar, M. Akhtar, A. Al-Hajry, M. Al-Assiri, G. Dar and M. S. Islam, *Chemical Engineering Journal*, 2015, **262**, 588-596.
49. M. F. Ehsan and T. He, *Applied Catalysis B: Environmental*, 2015, **166**, 345-352.
50. D. Chen and J. Ye, *Advanced Functional Materials*, 2008, **18**, 1922-1928.
51. F. Chen, Y. Cao, D. Jia and X. Niu, *Ceramics International*, 2013, **39**, 1511-1517.
52. P. Ji, B. Tian, F. Chen and J. Zhang, *Environmental technology*, 2012, **33**, 467-472.
53. S. Apte, S. Naik, R. Sonawane, B. Kale and J. Baeg, *Journal of the American Ceramic Society*, 2007, **90**, 412-414.
54. Q. Zhang, C. S. Dandeneau, X. Zhou and G. Cao, *Adv. Mater.*, 2009, **21**, 4087-4108.
55. R. Vinu and G. Madras, *Journal of the Indian Institute of Science*, 2012, **90**, 189-230.
56. S. Chakrabarti and B. K. Dutta, *J. Hazard. Mater.*, 2004, **112**, 269-278.
57. M. Shanthi and V. Kuzhalosai, 2012.
58. E. Yassıtepe, H. Yatmaz, C. Öztürk, K. Öztürk and C. Duran, *Journal of photochemistry and photobiology A: Chemistry*, 2008, **198**, 1-6.
59. A. B. Lavand and Y. S. Malghe, *International Journal of Photochemistry*, 2015, **2015**.
60. M. R. Hoffmann, S. T. Martin, W. Choi and D. W. Bahnemann, *Chem. Rev.*, 1995, **95**, 69-96.
61. A. Mills, R. H. Davies and D. Worsley, *Chem. Soc. Rev.*, 1993, **22**, 417-425.
62. M. Long, W. Cai, J. Cai, B. Zhou, X. Chai and Y. Wu, *The Journal of Physical Chemistry B*, 2006, **110**, 20211-20216.
63. H.-l. XIA, H.-s. ZHUANG, T. Zhang and D.-c. XIAO, *Journal of Environmental Sciences*, 2007, **19**, 1141-1145.
64. H. Seema, K. C. Kemp, V. Chandra and K. S. Kim, *Nanotechnology*, 2012, **23**, 355705.
65. Y. Wu, F. Xu, D. Guo, Z. Gao, D. Wu and K. Jiang, *Appl. Surf. Sci.*, 2013, **274**, 39-44.
66. A. Ye, W. Fan, Q. Zhang, W. Deng and Y. Wang, *Catalysis Science & Technology*, 2012, **2**, 969-978.
67. M. Vinothkannan, C. Karthikeyan, A. R. Kim and D. J. Yoo, *Spectrochimica Acta Part A: Molecular and Biomolecular Spectroscopy*, 2015, **136**, 256-264.
68. W. Dong, C. W. Lee, X. Lu, Y. Sun, W. Hua, G. Zhuang, S. Zhang, J. Chen, H. Hou and D. Zhao, *Applied Catalysis B: Environmental*, 2010, **95**, 197-207.
69. N. Karamat, M. N. Ashiq, M. F. Ehsan, S. Ijaz, I. Ali and I. H. Gul, *J. Alloys Compd.*, 2016, **689**, 94-106.
70. J. Saffari, N. Mir, D. Ghanbari, K. Khandan-Barani, A. Hassanabadi and M. R. Hosseini-Tabatabaei, *Journal of Materials Science: Materials in Electronics*, 2015, **26**, 9591-9599.

71. M. Bagheri, A. R. Mahjoub and B. Mehri, *RSC Advances*, 2014, **4**, 21757-21764.
72. B. Li, T. Liu, Y. Wang and Z. Wang, *J. Colloid Interface Sci.*, 2012, **377**, 114-121.
73. M. Pirhashemi and A. Habibi-Yangjeh, *Appl. Surf. Sci.*, 2013, **283**, 1080-1088.
74. B. Pant, H. R. Pant, N. A. Barakat, M. Park, K. Jeon, Y. Choi and H.-Y. Kim, *Ceram. Int.*, 2013, **39**, 7029-7035.
75. R. Saravanan, S. Karthikeyan, V. Gupta, G. Sekaran, V. Narayanan and A. Stephen, *Materials Science and Engineering: C*, 2013, **33**, 91-98.
76. M. Faisal, S. B. Khan, M. M. Rahman, A. Jamal, K. Akhtar and M. Abdullah, *Journal of Materials Science & Technology*, 2011, **27**, 594-600.
77. M. Goodarzi, S. Joukar, D. Ghanbari and K. Hedayati, *Journal of Materials Science: Materials in Electronics*, 2017, 1-16.
78. M. T. Uddin, Y. Nicolas, C. Olivier, T. Toupance, L. Servant, M. M. Müller, H.-J. Kleebe, J. r. Ziegler and W. Jaegermann, *Inorg. Chem.*, 2012, **51**, 7764-7773.
79. K. Yadav, M. Giri and N. Jaggi, *Res. Chem. Intermed.*, 2015, **41**, 9967-9978.
80. H. Liu, Y. Hu, X. He, H. Jia, X. Liu and B. Xu, *Journal of Alloys and Compounds*, 2015, **650**, 633-640.
81. S. Cho, J.-W. Jang, J. Kim, J. S. Lee, W. Choi and K.-H. Lee, *Langmuir*, 2011, **27**, 10243-10250.
82. K. Wang, J. Chen, W. Zhou, Y. Zhang, Y. Yan, J. Pern and A. Mascarenhas, *Adv. Mater.*, 2008, **20**, 3248-3253.
83. S. Cho, J.-W. Jang, J. S. Lee and K.-H. Lee, *Nanoscale*, 2012, **4**, 2066-2071.
84. W. Chen, N. Zhang, M. Zhang, X. Zhang, H. Gao and J. Wen, *CrystEngComm*, 2014, **16**, 1201-1206.
85. D. P. Steensma, *Archives of pathology & laboratory medicine*, 2001, **125**, 250-252.
86. A. Afkhami and R. Moosavi, *J. Hazard. Mater.*, 2010, **174**, 398-403.
87. X. Lin, Y. Mao, Q. Qi, C. Zhang, Y. Tian and Y. Chen, *Diagnostic pathology*, 2015, **10**, 174.
88. Y.-J. Cho, H.-i. Kim, S. Lee and W. Choi, *Journal of Catalysis*, 2015, **330**, 387-395.
89. X. Wang, W.-c. Peng and X.-y. Li, *International Journal of Hydrogen Energy*, 2014, **39**, 13454-13461.
90. S. Martha, D. Das, N. Biswal and K. Parida, *J. Mater. Chem.*, 2012, **22**, 10695-10703.
91. V. M. Daskalaki, M. Antoniadou, G. Li Puma, D. I. Kondarides and P. Lianos, *Environmental science & technology*, 2010, **44**, 7200-7205.
92. X. Zhang, H. Liu, W. Li, G. Cui, H. Xu, K. Han and Q. Long, *Catal. Lett.*, 2008, **125**, 371-375.
93. J. Xu and X. Cao, *Chem. Eng. J.*, 2015, **260**, 642-648.
94. L. Jia, D.-H. Wang, Y.-X. Huang, A.-W. Xu and H.-Q. Yu, *The Journal of Physical Chemistry C*, 2011, **115**, 11466-11473.

95.   T. Miwa, S. Kaneco, H. Katsumata, T. Suzuki, K. Ohta, S. C. Verma and K. Sugihara, *Int. J. Hydrogen Energy*, 2010, **35**, 6554-6560.

96.   J.-H. Yan, Y.-R. Zhu, Y.-G. Tang and S.-Q. Zheng, *J. Alloys Compd.*, 2009, **472**, 429-433.

97.   A. Pérez-Larios, R. Lopez, A. Hernandez-Gordillo, F. Tzompantzi, R. Gómez and L. Torres-Guerra, *Fuel*, 2012, **100**, 139-143.

98.   K. Byrappa and M. Yoshimura, *Handbook of hydrothermal technology*, William Andrew, 2012.

99.   A. Rabenau, *Angew. Chem. Int. Ed.*, 1985, **24**, 1026-1040.

100.   R. Roy, *J. Solid State Chem.*, 1994, **111**, 11-17.

101.   B. D. Cullity and J. W. Weymouth, *American Journal of Physics*, 1957, **25**, 394-395.

102.   D. P. Moecher, *Journal of Geoscience Education*, 2004, **52**, 5-9.

103.   J. Goldstein, *Practical scanning electron microscopy: electron and ion microprobe analysis*, Springer Science & Business Media, 2012.

104.   J. Goldstein, D. E. Newbury, P. Echlin, D. C. Joy, A. D. Romig Jr, C. E. Lyman, C. Fiori and E. Lifshin, *Scanning electron microscopy and X-ray microanalysis: a text for biologists, materials scientists, and geologists*, Springer Science & Business Media, 2012.

105.   R. D. Willis, F. T. Blanchard and T. L. Conner, *EPA. Washington, US*, 2002.

106.   D. B. Williams and C. B. Carter, in *Transmission electron microscopy*, Springer, 2009, pp. 3-22.

107.   L. Reimer, *Transmission electron microscopy: physics of image formation and microanalysis*, Springer, 2013.

108.   H. Förster, *Characterization I*, 2004, 2734-2734.

109.   H.-H. Perkampus and H.-C. Grinter, *UV-VIS Spectroscopy and its Applications*, Springer, 1992.

110.   R. Van Grieken and A. Markowicz, *Handbook of X-ray Spectrometry*, CRC Press, 2001.

111.   S. Brodowski, W. Amelung, L. Haumaier, C. Abetz and W. Zech, *Geoderma*, 2005, **128**, 116-129.

112.   R. Ahmed, L. Zhao, A. J. Mozer, G. Will, J. Bell and H. Wang, *The Journal of Physical Chemistry C*, 2015, **119**, 2297-2307.

113.   M. Gratzel, *nature*, 2001, **414**, 338.